TECHNICAL UNIVERSITY OF CARTAGENA

DEPARTMENT OF INFORMATION AND
COMMUNICATION TECHNOLOGIES

Graduate Thesis

Study and design of novel reflectarray configuration for space applications

AUTHOR: Aitor Correas Serrano

SUPVERVISOR: Alejandro Álvarez Melcón

CO-SUPERVISOR: Juan Sebastián Gómez Díaz

Cartagena, July 2015

Author	Aitor Correas Serrano
Author's email	aitor.correas@gmail.com
Supervisor	Alejandro Álvarez Melcón
Supervisor's email	alejandro.alvarez@upct.es
Supervisor	Juan Sebastián Gómez Díaz

Title	Study and design of novel reflectarrays for space applications
Título	Estudio y diseño de nuevos reflectarrays para aplicaciones espaciales

Abstract

Reflectarray antennas offer an attractive alternative solution to both reflector antennas and antenna arrays. These antennas have attracted significant attention in space applications thanks to their low mechanical complexity and their lack of a complex feeding network. Reflectarray antennas consist of a reflector antenna whose parabolic reflector is replaced by a planar surface. This reflectarray surface consists of isolated radiating elements, and it is illuminated by a feeder located away from the surface. These isolated radiating elements are pre-designed to manipulate the features of the radiated beam in terms of direction, beamwidth, polarization, etc. The key element of reflectarray beamforming is the phase shift introduced by each unit-cell, which is obtained by varying some of the geometrical parameters of the unit cell itself. The design of the reflectarray utilizes reflection phase design curves. Various elements have been used for the synthesis of reflectarrays, such as variable size microstrip patches of different forms and patches attached to stubs of different lengths at microwave frequencies, or subwavelength plasmonic resonator and composite configurations at near infrared and optical frequencies..

In this project we present the design of a reflectarray based on a novel substrate integrate waveguide (SIW) unit-cell configuration. First the phase delay required in each element is determined in order to achieve a reflecting surface that reflects a planar wave towards any desired direction, providing the physical dimensions of our reflectarray. Secondly we proceed to the complete design of a reflectarray cell using full-wave commercial software based on the finite element method (FEM). Our unit cell is simulated using periodic boundary conditions in order to approximate the conditions of the reflectarray, in which each unit cell will be surrounded by many others with similar features. In order to achieve the required phase delay in each unit cell we will use a multi-layer design in which the microstrip patches are attached to SIW stubs coupled by a slot. Lastly we present a Infinite Array Structure-Rectangular Waveguide Simulator (IAS-RWG) design which can be used to empirically test a prototype unit cell with periodic boundary conditions, thus testing the unit cell as if it was integrated in a realistic reflectarray located in free space.

Resumen

Los reflectarrays ofrecen una solución alternativa a las antenas reflectoras y los arrays de antenas. Este tipo de antenas ha suscitado considerable interés para su uso en aplicaciones espaciales debido a su baja complejidad mecánica y la ausencia de una red de alimentación compleja. Un reflectarray consiste en elementos radiantes aislados que son iluminados por un alimentador externo a la superficie. Estos elementos estan prediseñados para que ofrezcan un desfase particular al reflejar la radiacion incidente para manipular características del haz radiado tales como la dirección, ancho de haz, polarización, etc. El elemento clave para la formación de haz es el desfase introducido por cada celda unidad, que se obtiene variando parámetros geométricos de ésta. Para diseñar los reflectarrays se hace uso de gráficas que relacionan parametros físicos de la celda con el desfase de la onda reflejada. En el pasado, se han utilizado varios elementos para la síntesis de reflectarrays, tales como parches microstrip de tamaño variable o parches acoplados a stubs de diferente longitud para microondas, o resonadores plasmónicos y configuraciones compuestas en infrarrojos y frecuencias ópticas. En este proyecto presentamos el diseño de un reflectarray basado en celdas unidad implementadas utilizando guias de onda integradas en substrado (SIW). En primer lugar calculamos el desfase necesario en cada elemento para conseguir un frente de onda reflejado de onda plana en cualquier dirección deseada partiendo de los parámetros físicos del reflectarray . A continuacón procedemos con el diseño completo de la celda unidad utilizando software de onda completa basado en el metodo de los elementos finitos (FEM). La celda unidad se simula utilizando condiciones de contorno periódicas para aproximar las condiciones de trabajo de la celda en el reflectarray, en el cual cada celda esta rodeada de muchas otras de similares características. Para conseguir el desfase necesario en cada celda usaremos un diseño multicapa en el cual los parches de microstrip se encuentran acoplados a stubs implementados en SIW mediante una ranura. Por último presentamos el diseño de un Rectangular Waveguide Infinite Array Simulator (RWG-IAS) que puede ser utilizado para testear un prototipo de celda unidad en condiciones de contorno periodicas, consiguiendo resultados similares a los que se obtendrían si la celda estuviese integrada en un reflectarray real en espacio libre.

Degree	Grado en Ingeniería en Sistemas de Telecomunicaciones
Department	Information and Communication Technologies
Submission date	July 2015

Contents

Chapter 1

Introduction

Communications satellites are formed by various subsystems, among these, the antenna subsystems are specially important. An antenna transforms guided waves into radiated waves which are propagated through the air (or the vacuum), and vice-versa. This transformation happens both ways depending on whether the antenna is transmitting or receiving. The antenna subsystem must be correctly designed in order to fulfill the technical specifications of the communications satellites and also enabling an easy transport and orbital deployment. The space available at the launching vehicle is limited and the total cost significantly increases versus the mass and volume of the different subsystems, which imposes important constrains in the design of space antennas. Traditionally, parabolic reflective antennas, as well as antenna arrays, have been the most popular solutions for space satellites, as they generally fulfill these requirements better than other technologies. A good alternative for parabolic reflectors on space satellites are the reflectarray antennas [1]. A printed reflectarray antenna consists of a planar array of printed radiating elements that introduces a certain phase shift between elements to produce a collimated or a shaped beam when it is illuminated by a feed [2]. This phase shift is equivalent to the phase shift introduced by the physical parabolic shape of a traditional reflector. Over the past years, reflectarray antennas have attracted considerable attention thanks to the development of sophisticated printed technologies.

With the rapid advancement in fabrication technologies, reflectarray antennas offer a potentially attractive alternative solution to both reflector antennas and antenna arrays [3]. Figure 1.1a shows a diagram of a modern reflectarray, made by copper patches on a dielectric substrate backed up by a ground plane. A real

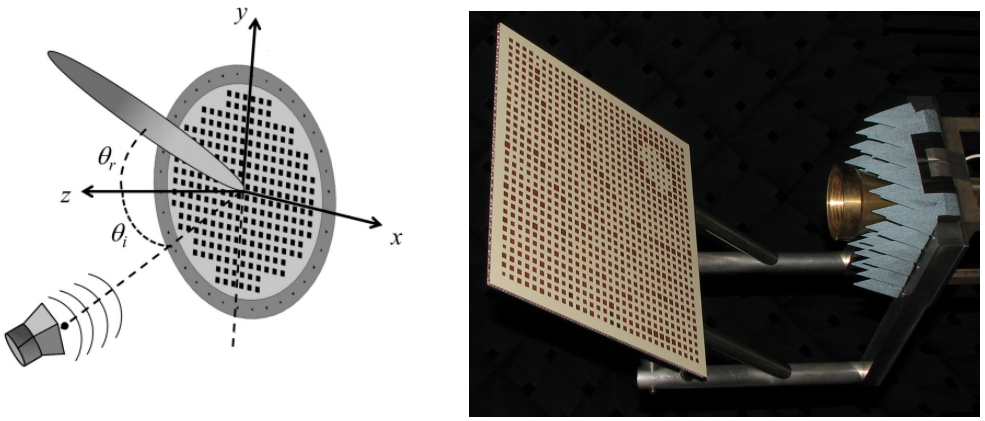

(a) **(b)**

Figure 1.1: Reflectarray antenna examples: (a) shows printed reflectarray 3D diagram; (b) shows a real reflectarray structure being measured at an anechoic chamber. Figures from [1, 4]

reflectarray structure being measured in an anechoic chamber is shown in figure 1.1b.

Reflectarray antennas are less expensive and structurally better for satellite communications due to their planar form, which allows an easy deployment while limiting the total mass and volume. The main downside of reflectarray antennas is the narrow band at which they operate, a limitation inherent to the technology, but that can be mitigated using different methods, such as stacked patches or True Time Delay (TTD) techniques [5], which will be discussed along this project. Even with such a limitation, reflectarray antennas remain as a solid candidate to take over antenna subsystems on spatial applications, as they lack complex feeding systems (in contrast to printed antenna arrays), allow electrical beam scanning and have a convenient structure for spacial applications (as opposed to parabolic reflectors). As a relatively new technology with high potential, reflectarrays appear as an interesting field to research in order to minimize de limitations aforementioned.

In this context, this project tries to bring a certain degree of innovation into reflectarray design by applying novel technologies. First, the existing technologies regarding reflectarray design, as well as the common procedures for designing reflectarrays are shortly reviewed in chapter 2. Later an alternative structure making use of substrate integrated waveguide (SIW henceforth) for reflectarrays based on aperture coupled patches is proposed, designed and simulated using the full wave software HFSS from Ansoft (chapter 3). Lastly, a model to empirically verify the

correct operation of the designed elements based on the Rectangular Waveguide-Infinite Array Simulator (RWG-IAS) is proposed as a follow up for this project (chapter 4). The whole project undertakes the comprehensible electrical design of a complete reflectarray structure for any given main beam direction.

Chapter 2

Reflectarray Analysis and design techniques

In this chapter we briefly review the common procedures for designing reflectarrays, including both unit cell design and general reflectarray design, namely the phase shift distribution needed for each element of the reflectarray surface. We also introduce a number of concepts related to reflectarray design such as (TTD), Floquet's theorem and periodic boundary conditions (PBC), with the aim of offering a better understanding of this project's methodology, designs, results and conclusions.

A printed reflectarray is a planar structure formed by an array of printed passive radiating elements that produce a beam when illuminated by a feed external to the surface. The characteristics of the scattered wave are determined by the phase shift introduced by the radiating elements mentioned, usually referred to as 'unit cells' of the reflectarray. The incident fields on the reflectarray elements are considered as plane waves with a phase proportional to the distance from each element to the feeder antenna, which is located in the far field. In order to convert the incident wave radiated by the horn into a focused beam, the field must be reflected from each element with an appropriate phase shift. This phase shift is adjusted independently for each element to achieve the phase difference between elements required to focus the scattered beam towards any desired direction, as is known from classic phased array theory. [6].

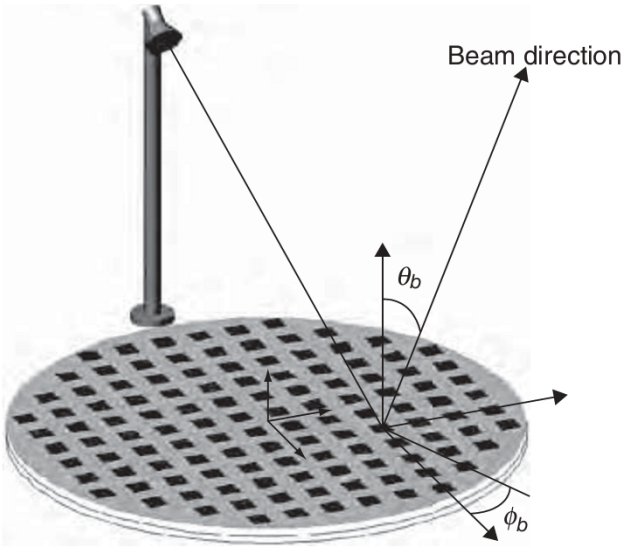

Figure 2.1: Typical geometry and coordinate system used on reflectarray antennas. Reproduced from [3].

2.1 Phase shift distribution

The phase shift distribution will control the scattered beam characteristics, that is, the reflectarray behaviour as a reflective antenna. Because of this, it is a crucial step in reflectarray design to compute this phase shift distribution accordingly to each design requirements. This section introduces a set of expressions to determine the phase shift distribution necessary for a reflectarray to radiate in any desired direction. This set of expressions can be found in [3].

Considering the coordinate system detailed in figure 2.1 , the progressive phase distribution on the reflectarray surface that produces a beam in the direction (θ_b,φ_b), as known from array theory, is expressed as

$$\phi(x_i, y_i) = -k_0 sin\theta_b cos\varphi_b x_i - k_0 sin\theta_b sin\varphi_b y_i \tag{2.1}$$

where $k_0 = \frac{\omega}{c}$, ω is the operating frequency and c is speed of light in vacuum; x_i and y_i are the coordinates of element i. On the other hand, the phase of the reflected field at each reflectarray element is equal to the phase of the incident field, as a result of propagation from the feed, plus the phase-shift introduced by each cell. This writes:

$$\phi(x_i, y_i) = -k_0 d_i + \phi_R(x_i, y_i) \tag{2.2}$$

where ϕ_R (x_i,y_i) is the phase shift for element i and d_i is the distance from the

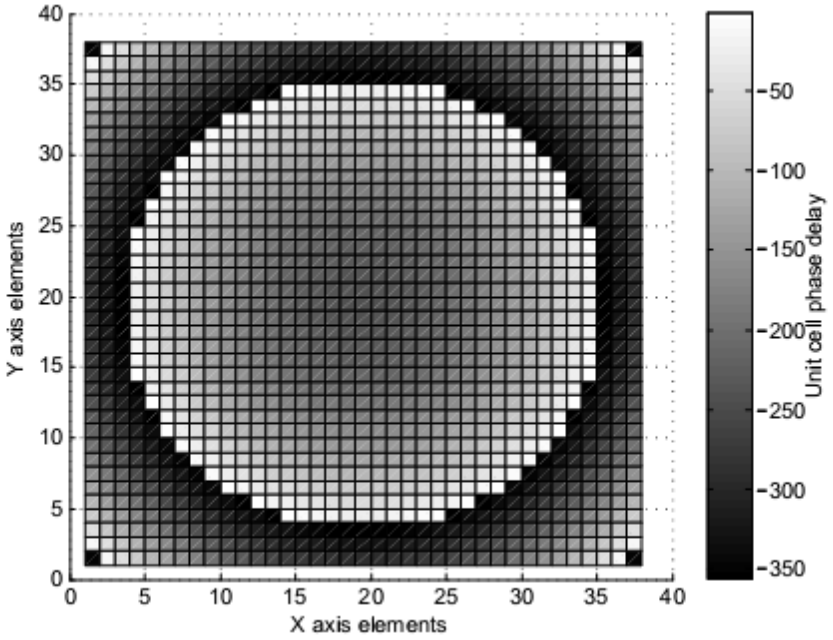

Figure 2.2: Phase delay required for each unit Cell on a 38 × 38 broadside reflectarray with centered feed.

phase center of the feed to the cell. From expressions (2.1) and (2.2), the phase shift required at each element is obtained:

$$\phi_R = k_0(d_i - (x_i cos\varphi_b + y_i sin\varphi_b)sin\theta_b) \tag{2.3}$$

Where φ_b and θ_b indicate the main beam direction, as shown in figure 2.1. Making use of (2.3) we can easily compute the phase shift required at each unit cell for a radiated beam in any desired direction. Note that factors such as the feed position or the separation between unit cells or spacing, affect the phase distribution of the reflectarray.

Figure 2.2 shows the required phase shift on a circular reflectarray of 38 × 38 elements with the feed centered that produces a pencil beam in a direction normal to the surface. The feed can also be positioned outside of the reflectarray reradiated wave main direction in order to avoid blocking the view. An example of the phase distribution needed in one of these cases is shown in figure 2.3. For reflectarray design, the phase of the reflection coefficient must be adjusted in each element to match theses phases. The phase-shift at figures 2.3 and 2.2 is achieved by varying one of the geometrical parameters in the reflectarray elements.

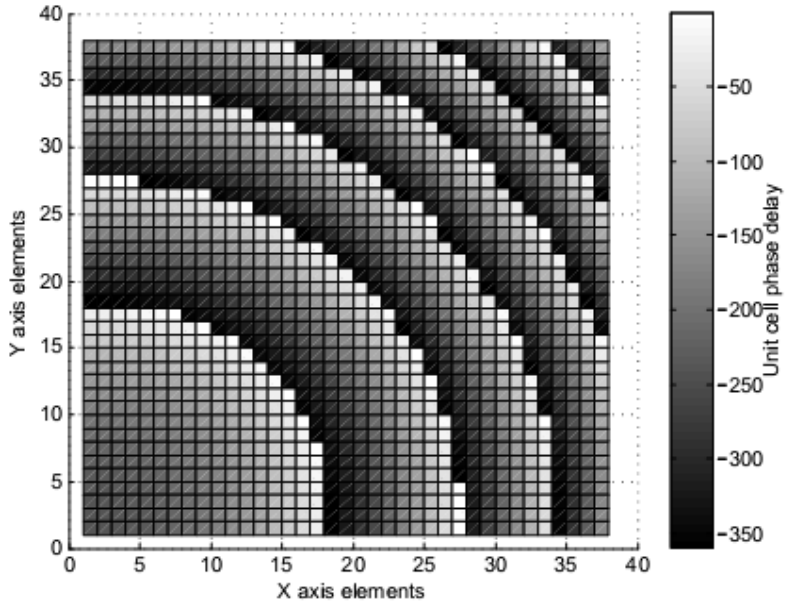

Figure 2.3: Phase delay required for each unit Cell on a 38×38 broadside reflectarray with the feed positioned in the down-left corner.

2.2 Element spacing and grating lobes

Another factor to take into account when designing reflectarrays and reflectarray elements is the spacing between unit cells in the planar surface of the reflectarray. For any array of antennas, including reflectarray structures, if the spacing is not correctly chosen, grating lobes will appear in the radiating pattern of the antenna. Grating lobes result on wasted energy and thus must be avoided whenever possible.

Grating lobes occur in uniformly spaced arrays when the element spacing is too large. It also depends on the incident angle as well as on the main beam directions (grating lobes occur easier the more inclined the main beam direction is). For elements located toward the edge, the wave's incident angles from the feed will usually be larger and thus these elements will determine the spacing of all the reflectarray elements (that is if the same spacing is used for the whole reflectarray, which is the usual case for ease of design and fabrication). The theoretical element spacing requirement should be governed by the following conventional array equation [3]:

$$\frac{d}{\lambda_0} \leq \frac{1}{1+\sin\theta} \tag{2.4}$$

where **d** is element spacing, λ_0 is the wavelength in vacuum and θ is either the

incident angle from the feed or the main beam tilt angle from the broadside direction, whichever is larger. Offset fed reflectarrays are more prone to grating lobe formation if element spacing is much larger than 0.5 λ_0. When element spacing is below $0.5\lambda_0$ no grating lobes will appear. More detailed information about the significance of grating lobes, as well as when an why they appear, can be found at [6]

2.3 Floquet's theorem

For the analysis of arrays with a large number of unit cells, analysis techniques to calculate the mutual coupling of all the elements are too costly. For this cases, the infinite array model is usually used and, by applying periodic boundary conditions (PBC) based on Floquet's theorem, the analysis is reduced to only one periodic cell.

In this section we explain Floquet's theorem, as well as the periodic boundary conditions (PBC) that derive from it, as they are used in the simulation of unit cells to approximate infinite array environments. Full demonstration of Floquet's theorem in the case of electromagnetic waves in periodic structures can be found in [7, 8]. Floquet's theorem describes the electromagnetic fields on an infinite, periodic structure when affected by an electromagnetic wave.

The electromagnetic fields in an infinite periodic structure consist of a superposition of modes which are called Floquet's modes. These modes are different solutions for Maxwell equations and can be expressed as follows:

$$U(r) = U_p(r)e^{-\gamma r} \tag{2.5}$$

being

$$U_p(r + R) = U_p(r) \tag{2.6}$$

where U (r) is any field component, R the position vector on the surface, $U_p(r)$ a periodic function in space (different for each Floquet's mode) and γ the equivalent propagation vector (different for each Floquet's mode). So, the field is the same in all cells of the structure, except for a propagation factor $e^{-\gamma r}$, where $Re[\gamma]$ is not necessarily zero. In other words, the Floquet's mode field can be seen as a travelling wave within the surface with $e^{-\gamma r}$, with possible surface losses, modulated in space by the periodic function Up (r). Another form of this theorem can easily be obtained

from (2.5) and (2.6) and writes:

$$U(r+R) = U_p(r)e^{-\gamma R} \tag{2.7}$$

If we assume the periodic structure to be illuminated by a plane wave (as it is the case in reflectarrays), we observe again from the form (2.7) of Floquet's theorem that the total fields in two successive cells of the structure only differ by the propagation factor $e^{-\gamma R}$, and that this propagation factor is the same for all cells. As the structure is infinite and illuminated by a plane wave, the only possible total field propagation factor between successive cells is that of the incident plane wave. Mathematically, this writes:

$$\gamma R = j(kR + 2p\pi), \qquad p \in \mathbb{Z} \tag{2.8}$$

Note that under illumination by a plane wave, the real part of the transverse components of γ is zero. This is due to the fact that the infinite structure being illuminated by an infinite plane wave carries a field that do not decay in any direction. Thus, Floquet's theorem becomes in this case:

$$U(r+R) = U_p(r)e^{-jkR} \tag{2.9}$$

In summary, in the case of a 2-D structure excited by an impinging plane wave, the Floquet's propagation vector γ in 2.5 only depends on the incident plane wave and is known. However, the form of the fields in a unit cell, or $U_p(r)$, depends on the structure of the cell itself.

2.3.1 Periodic boundary conditions waveguide (PBC-WG)

As a result of Floquet's theorem, the unit cell of the periodic structure can be seen as a waveguide with its axis in the z direction and its lateral walls subject to PBCs, as illustrated in Figure 2.4. The PBCs consist in enforcing that the field is the same on two opposite walls, except for a phase shift function of the frequency and incident wave angle. This structure referred to here as the periodic boundary conditions waveguide (PBC-WG).

By using PBC-WG we 'force' Floquet's theorem into the unit cell, imposing the electromagnetic fields occurring in the unit cell to be 'replicated' around it, except for a phase shift function of the frequency and incident wave angle. Periodically repeating the fields occurring in the unit cell is the same as considering an infinite

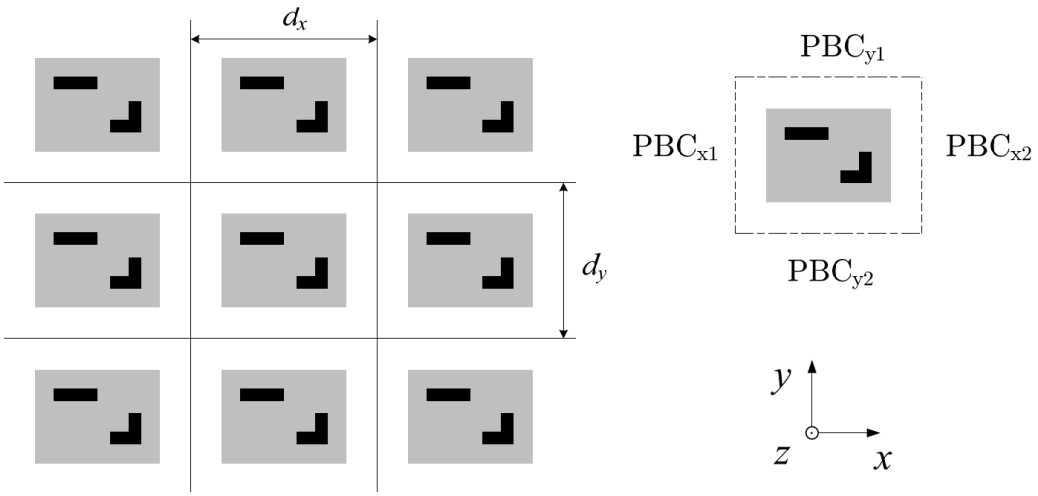

Figure 2.4: Infinite periodic structure model using PBC-WG. The unit cell is repeated by translation, creating an array environment for simulation. Reproduced from [7]

grid composed by the same unit cells. By doing so it is possible to simulate a single unit cell element in conditions close to that of the full reflectarray affected by a planar wave. With this we manage to achieve valid simulation results without needing to simulate a full reflectarray structure. Thus, the PBC-WG approach can be employed to compute the reflection phase that will determine the direction of the radiated beam in a reflectarray.

For normal incidence, it is theoretically equivalent to simulate the structure with PBCs and pairs of confronted PEC/PMC boundaries, as it is not needed to apply the phase delay between walls that PBC conditions do (phase delay is 0 in this case). We will refer to the latter simulation setup as the perfect electric/magnetic conductor waveguide (PECPMC-WG).

PECPMC simulations are much less costly than PBC, but only represent normal incidence of the wave and symmetry in both X and Y axis of the unit cell plane is required, as those boundary conditions don't replicate the fields, but mirror them. If this condition is not met, PECPMC-WG will not result on a periodic array simulation.

2.4 True Time Delay

In this section we introduce the concept of true time delay (TTD from this point onwards) as a way to improve the bandwidth of reflectarray structures. A more detailed explanation and demonstration can be found at [5]

As explained earlier on this work, the most severe drawback in reflectarray antennas is their narrow-band performance, and much effort has been made in recent years in order to overcome this limitation [9, 10]. Reflectarray bandwidth is limited mainly by two different factors. The first is the narrow frequency band of the radiating elements; the second is the differential spatial phase delay happening as a result of the different paths from the feed to each point on the wave front of the reradiated beam.

Different types of reflectarray elements have been proposed to improve the element bandwidth in printed reflectarrays such as stacked rectangular and ring patches. Some of the proposed structures are shown in figure 2.6.

Usually, any required phase shift value that satisfies the phase shift distribution of a certain reflectarray design can be achieved within a range of 360°. When frequency varies out of the central one, a phase error proportional to the differences in path length appears, producing a deterioration of the reflectarray performance both in beam shape and gain.

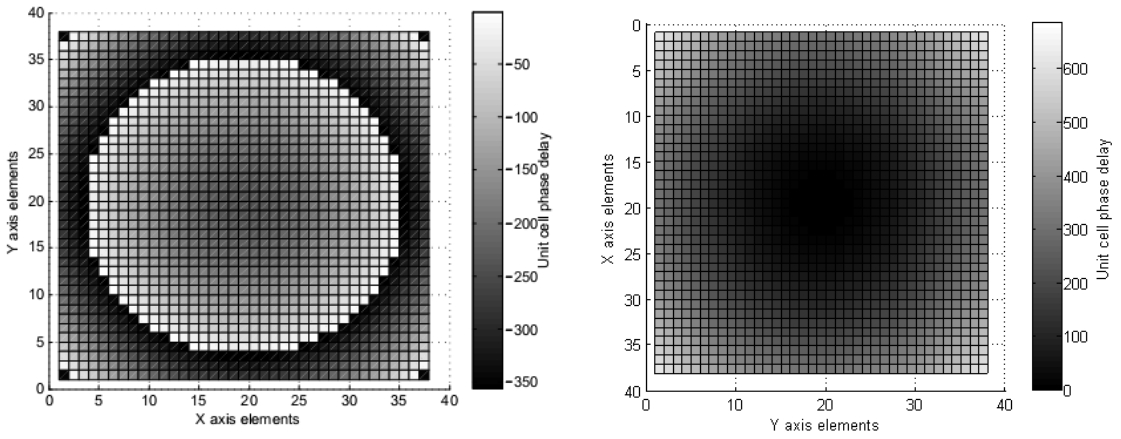

(a) **(b)**

Figure 2.5: Phase delay required for each unit Cell on a 38 × 38 broadside reflectarray with centered feed; (a) shows the phase delay without TTD, (b) shows the phase delay with TTD.

Parabolic reflector antennas use the physical geometry to reflect spherical waves arriving from the feed to form a planar wave front. This phase equalization is independent of the frequency, and it is equivalent to the true-time delay (TTD) technique, as it is called in phased arrays. In contrast, printed elements on reflectarrays are normally used for phase-shift compensation in a limited 360° phase range.

This phase-shift limitation to 360° can be removed to improve the bandwidth of reflectarrays. Stubs of variable length attached to rectangular patches, in long enough, can introduce a TTD. The available space for transmission lines on the reflectarray becomes the main limitation when implementing True Time Delay.

The improvement of bandwidth using true-time delay phase compensation in reflectarrays is demonstrated in [5]. There, a significant improvement in bandwidth is demonstrated when TTD is used.

2.5 Reflectarray design and unit cell structures

The phase shift introduced by the unit cells is their single most important parameter as it will determine the behaviour of the full reflectarray structure, as it controls the characteristics of the scattered wave. For this reason it is extremely important that the phase introduced by the unit cells can be set to any needed value when constructing the reflectarray, with as little error as possible. As a result, designs with more predictable phase shifts and linear responses versus the dimensions of some geometrical parameter are preferred over steep phase curves that can lead to higher phase errors caused by imprecisions during construction or changes in the operating frequency (which result on a change on the electric dimensions of the unit cell).

The phase shift at each element controlled by varying geometrical parameters in the reflectarray unit cell. Multiple ways to control the phase shift introduced by the unit cells have been studied [11, 12]. Some of these are:

- Printed dipole unit cells (figure 2.6a). In this configuration, the dipoles resonate at the design frequency and the phase shift of each element is controlled by varying the length of the dipole. It is the simplest structure but the phase shift range obtainable by varying the dipole length is about 330°. Variations

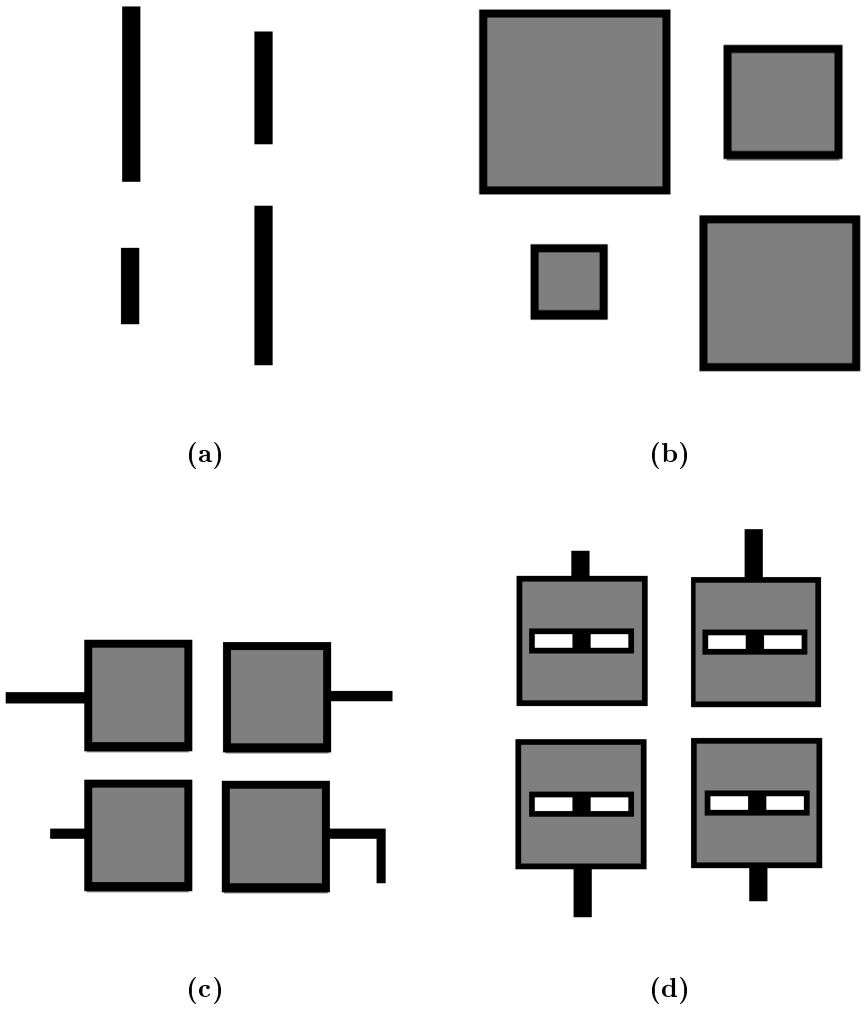

Figure 2.6: Simplified top down view of different types of existing reflectarray unit cell structures: (a) shows printed dipole unit cells of different length for different phase shift; (b) shows single layer printed patch structure for different phase shifts; (c) shows printed patches with microstrip stubs of variable lengths for different phase shifts directly connected to them; (d) shows apperture coupled patches for different phase shifts.

using multiple dipoles with different lengths/orientation have been studied to improve the performance of this type of unit cells.

- Printed microstrip patch unit cells (figure 2.6b). Similar to the printed dipole ones, the patches resonate at the design frequency and the phase shift is controlled by changing the dimensions of the patch. Its phase is limited as well to around 330°. Unit cells with stacked patches and different patch shapes have been proposed in order to increase bandwidth and general performance

of these unit cells.

- Printed microstrip patches with microstrip stubs directly connected to them (figure 2.6c). The phase shift on the unit cell will depend on the length of the stub, often needing to shape it with specifically to fit into the reflectarray surface. The phase range will depend on the stub maximum possible length and will often surpass 360°. The shortcomings of this technique are the limited space, which limit the maximum phase range of the unit cell, and the radiating loses due to the shape of the microstrip stub and might affect the radiating pattern.

- Printed patches coupled to a stub through a slot, also referred to as aperture coupled patches (figure 2.6d). In this type of unit cell every patch share the same dimensions and the phase shift is introduced by a stub. The resultant phase shift introduced by the element is proportional to the length of the stub. Traditionally, microstrip technology has been used to implement said stubs. The phase range on this structure depends directly on the stub length, being possible to surpass the 360° limit, which permit the implementation of TTD

Figure 2.7 shows the variation on the phase-shift for different values of the design geometrical parameter and different frequencies around the design frequency (in this case 30 GHz). Phase shift introduced by single layer resonating elements with no delay stubs, such as printed microstrip patches or dipoles, is not linear versus the changing dimension of the design geometrical parameter. Figure 2.7a shows the phase shift introduced by a single layer printed microstrip patch unit cell, which is in clearly not linear. Phase range is also restricted to around 330°. On the contrary, the phase shift introduced by elements which add phase delay with stubs is more linear and the phase range is usually above 360°, as can be seen in figure 2.7b, which corresponds to the phase delay introduced by an aperture coupled patch unit.

In general, for the design of any reflectarray, any possible value of phase shift must be implemented by varying one parameter in the unit cell, such as the patch size (fig. 2.7a) or stub length(fig. 2.7b). One of the most important parts of the reflectarray analysis and design is the characterization of the unit cells, that is, for a given geometry of the reflectarray element, to accurately predict the phase shift and dissipative losses. The design of a unit cell for a reflectarray, with a

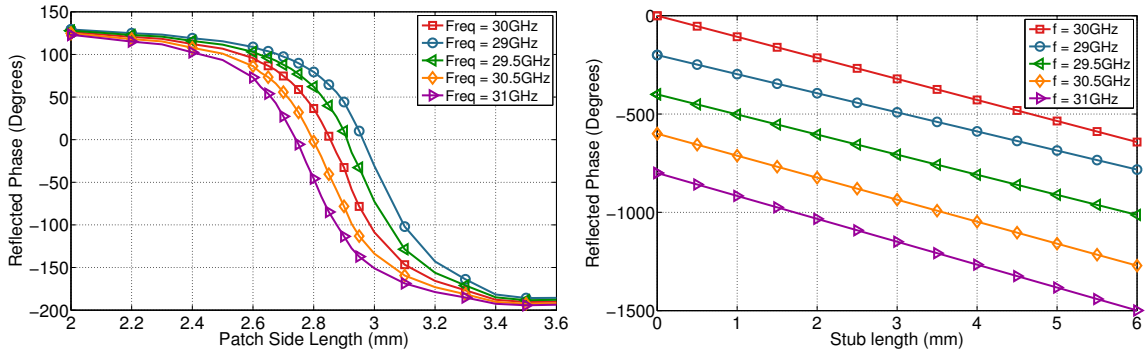

(a) **(b)**

Figure 2.7: Phase shift introduced by different unit cell structures versus the variable geometrical parameter: (a) shows the phase shift introduced by a single layer printed microstrip patch unit cell; (b) shows the phase shift introduced by an aperture coupled patch unit cell.

complete prediction of the phase shift and dissipation of each element in relation of its dimensions, is the main focus of this project.

The most common approach for the analysis and design of reflectarray antennas is based on the use of design curves relating the phase of the reradiated field with a certain geometrical parameter of the reflectarray element assuming normal incidence, like the curves shown in figure 2.7. This assumption is valid for the central elements of the centered fed reflectarray, that is for angles not too far from normal incidence. As the largest fraction of the incident power is reflected by the central part of the reflectarray, the normal incidence assumption can provide good predictions for center fed reflectarrays.

For the analysis of arrays with a large number of unit cells, analysis techniques to calculate the mutual coupling of all the elements are too costly. For this cases, the infinite array model is usually used and, by applying periodic boundary conditions (PBC) based on Floquet's theorem, the analysis is reduced to only one periodic cell [13]. This technique takes into account the mutual coupling between identical elements and provides good predictions of each element in the array environment. The analysis of the reflectarray element using the infinite array approach is very efficient, as well as being accurate in characterizing the reflectarray elements [2]. This technique is specially accurate for elements that introduce the phase shift with stubs , as all the radiating patches are exactly the same and only the stub length varies from one unit cell to the others. In this case the infinite array approach will

be very accurate because the coupling produced by the stubs is less significant.

2.6 Phase shifter and aperture-coupled patches

In the previous section we introduced aperture coupled patches as one of the possible structures for reflectarray unit cell design. Usually, in this configuration, each stub is made up of an open-ended length of microstrip line on the opposite side of the ground plane, which is electromagnetically coupled to the radiating patch by an aperture in the ground plane as shown in 2.8.

When the plane wave coming from the feed resonates with the square patch, it is coupled to the microstrip line on the bottom and propagates until reaching the open circuit extreme where it is reflected, coupled, and reradiated by the patch. As a result, the phase shift introduced by the element if the patch doesn't add extra phase shift will be $2\beta l$, where β is the phase propagation constant and l is the length of the microstrip stub.

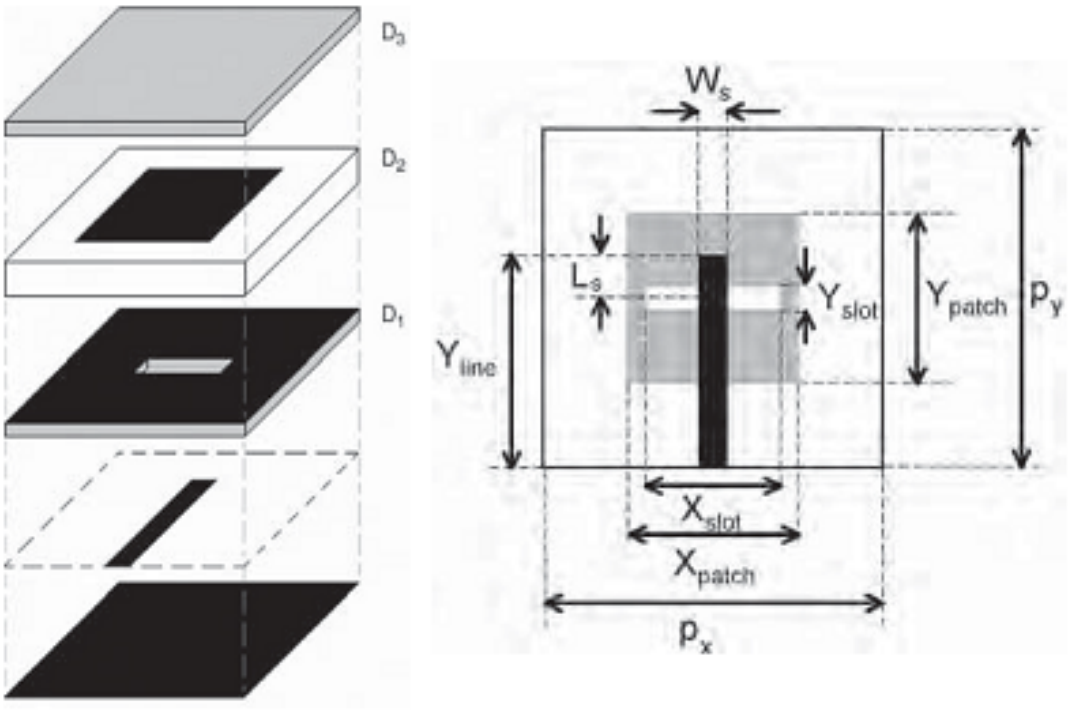

Figure 2.8: Aperture-coupled unit cell for reflectarray. Patch, slot and phase delay stub are the main components of this structure. On the left, layered view of the component. On the right, top view of the same unit cell. Figure reproduced from [3].

The aperture-coupled element must be designed in order to achieve a linear phase response in a range larger than 360° in order benefit from the TTD technique. For the design of the phase shifter, the line underneath the aperture is considered as two segments. The first one is a stub of a fixed length, which is adjusted to match the radiating element; the second is the variable length stub used to add the required phase delay for each unit cell.

First the aperture-coupled radiating element must be designed to achieve a good match between the line and the patch, considering a microstrip feed line as in the case of conventional active planar arrays. All the geometrical parameters, such as dielectric materials, thickness, dimensions of the aperture, patch, and fixed stub, have to be determined using a simulation tool. According to the reciprocity theorem, by achieving a good matching with the active radiating patch structure, a equally good matching will be obtained when functioning as a passive radiating element, as the fields resonating in the patch will be coupled into the stub and viceversa.

Once the element is designed to achieve a good matching, the curves of phase shift are obtained simulating the structure functioning as a passive reflectarray element, ideally using PBCs and repeating the simulation for various values of phase delay stub length. By doing so we obtain the curves of phase shift versus stub length which, as commented earlier on this chapter, is the final aim when designing unit cell structures.

Chapter 3

Unit Cell Design

3.1 Introduction

The aim of this chapter is to fully design a functional reflectarray unit cell based on the aperture-coupled patch model, utilizing SIW technology and TTD to optimize the design.

For the design of the radiating element and for the computation of the phase-shift curves, it is preferable to use a full-wave simulation tool assuming an infinite array model. For this project, full wave simulator HFSS from Ansoft is used. Since the apertures and patches are identical, and the reflectarray usually comprises a very large number of elements, the reflectarray can be considered as a periodic array, with the exception of the stubs of different lengths. The coupling between the stubs is ignored, as it is less important (especially when using SIW technology for the stub implementation, as the coupling between stubs will be even lower than with microstrip stubs). A comprehensible explanation of the design process followed in this chapter can be found at [14, 3, 15].

3.2 SIW technology on reflectarray unit cell design

The unit cell structure which will be used in this project consists on an aperture-coupled structure. Although the common technique consists on using open ended microstrip stubs, in this project a novel solution using SIW stubs is proposed. SIW technology [16] has lesser conductor losses at high frequency than microstrip technology, and allows for simpler multi-layer structures for each element of the reflectarray.

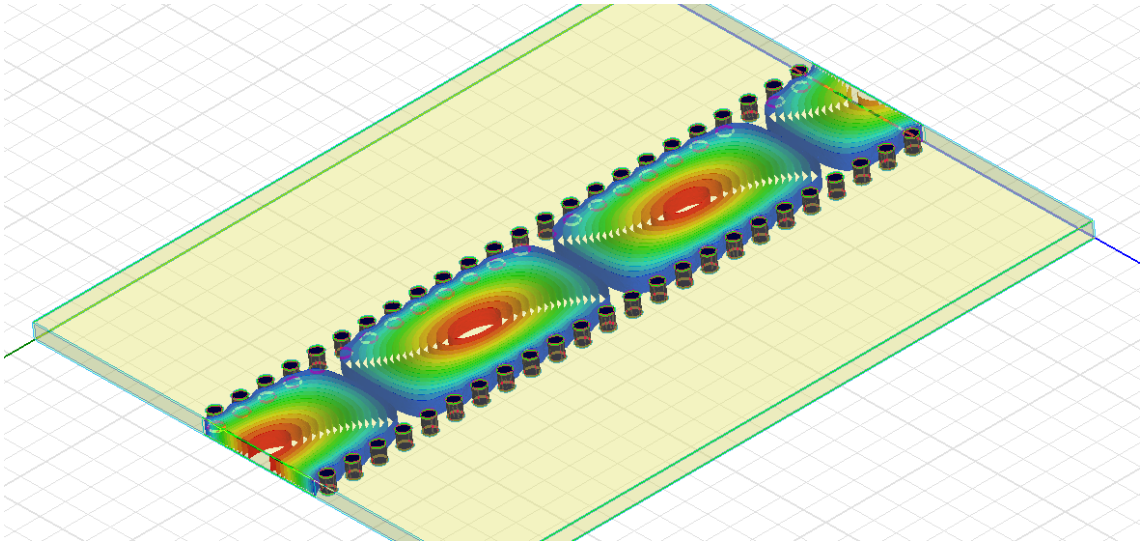

Figure 3.1: Fields propagated through a Substrate Integrated Waveguide functioning at 30 GHz. The metal vias function as side walls, confining the power. Only propagates TE_{m0} modes.

SIWs are integrated waveguide-like structures fabricated by using two rows of conducting cylinders or slots embedded in a dielectric substrate that electrically connect two parallel metal plates. SIW structures exhibit propagation characteristics similar to those of rectangular metallic waveguides, provided that the metallic vias are closely spaced and radiation leakage can be neglected. In SIW structures, only TE_{m0}, with m = 1,2,... modes can be propagated. TM modes are not supported due to the gaps between the metal bias.

Even though the losses in SIW structures are lower that those of microstrip lines, they are still higher than the losses at conventional waveguides. This is due to the dielectric propagating losses as well as the low dielectric thickness commonly used for this structures, way lower than the dimensions of the usual rectangular waveguide. Figure 3.1 shows the simulated fields propagating through a SIW structure. More detailed information about SIW technology waveguides, circuits and antennas can be found in [16]

A reflectarray element using SIW technology reduces the conductor losses at microwave and millimeter waves compared to microstrip transmission lines, when true-time delay is required. Compared to patches aperture-coupled to microstrip lines, SIW technology simplifes the multi-stack structure by reducing in one the amount of dielectric layers needed; and eliminates the back radiation, as the wave is completely guided, without leakage of energy. Theoretically it is possible to stack

as many layers as needed with ease by using SIW technology for the stubs instead of microstrip. By using SIW each layer consist of two ground planes (top and bottom of the SIW), with a coupling slot on each ground plane (except the last one) to achieve coupling between layers. This structure allows to stack layers, being the bottom of one SIW the top of the next. On the contrary, when using microstrip technology it is not possible to stack layers with ease, as the structure becomes more intricate and voluminous. Even when only using one layer for the phase delay stub, SIW based unit cells require one less dielectric layer than the equivalent microstrip implementations, resulting in a cheaper and much easier to fabricate structure.

The first layer consists on a square patch of fixed dimensions over a dielectric. Below that there will be a slot on a ground plane in order to achieve coupling with

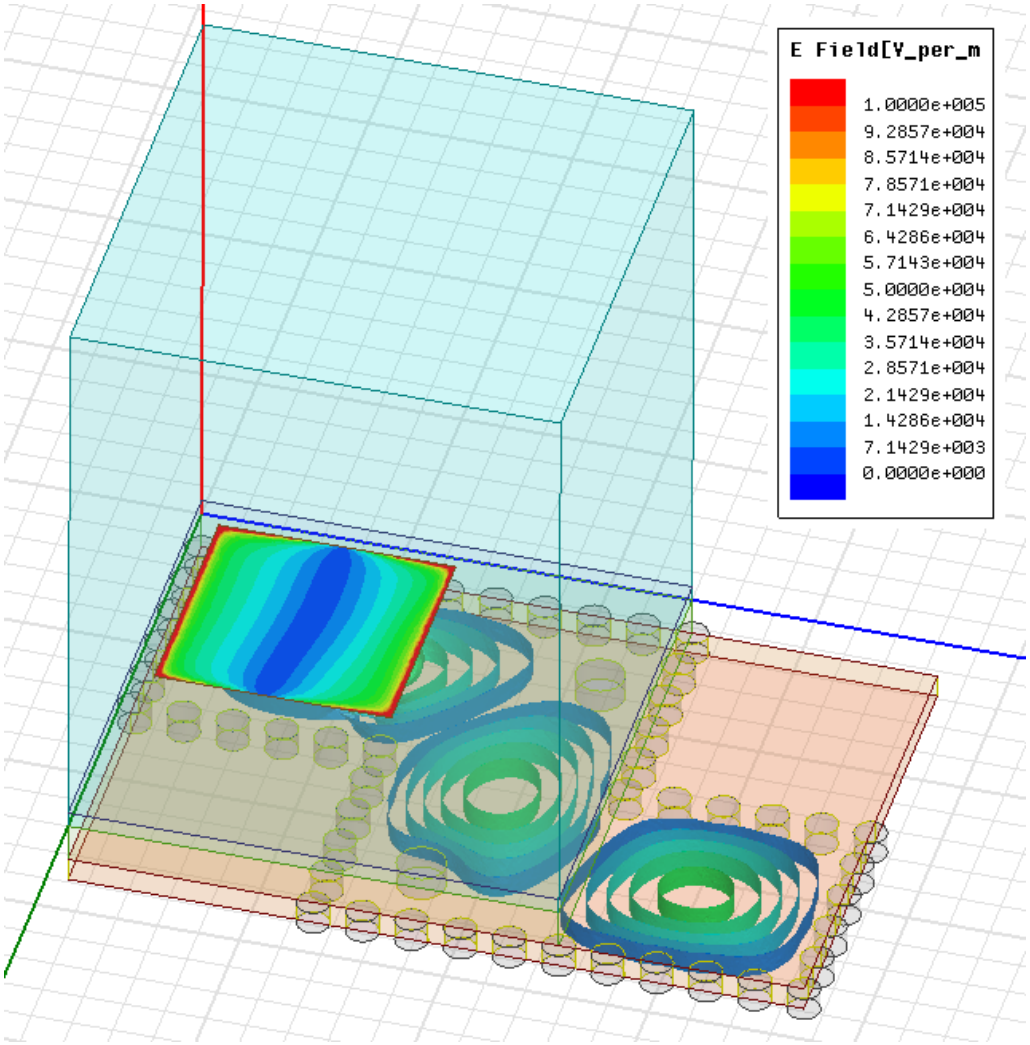

Figure 3.2: Proposed aperture-coupled patch unit cell using SIW technology to implement the phase-shift variable stubs.

a transmission line stub, which will be located directly under the slot. Since every patch in the reflectarray will have the same dimensions, the required phase delay will be introduced by stubs of different lengths under each unit cell.

As stated in chapter 2, this structure has been demonstrated to be effective in numerous works before this. In this work we propose as novelty the use of SIW (Substrate Integrated Waveguide) technology in order to implement this stub.

Figure 3.2 show the proposed unit cell design for this chapter. The design process, as well as the relevant results will be presented in this chapter.

3.3 Proposed structure and design

It is important to properly understand the structure of the unit cell and the importance of each of its parts. First, the square patch will be of fixed, invariable dimensions for each and every unit cell along the reflectarray. The dimensions will be decided in order to achieve coupling between the incident wave from the feed and the patch. This patch is placed on top of a dielectric, preferably of low dielectric constant. Below there is a slot on a metallic sheet in order to couple the electromagnetic fields on the patch with the stub below it. By varying the length of the stub we can easily achieve a wide range of phase delays on each patch. As said before, this stub is implemented using SIW technology. For this SIW a high dielectric constant will be used in order to achieve larger values of phase propagation constant and thus maximize the phase delay obtained in each reflectarray cell.

The aim of this chapter is to design an optimized fully working unit cell for a reflectarray operating at the frequency of 30GHz. In order to do so, full wave simulator HFSS is used. This unit cell is simulated using periodic boundary conditions (PBC) waveguide setup in order to mimic the conditions of the reflectarray, in which each unit cell will be surrounded by many others of the same characteristics, as explained in section 2.3.

The structural characteristics of the design are as follows:

- Design based on aperture coupled patch functioning at 30 GHz central frequency.
- Unit cell size (spacing between elements of the reflectarray) of 6 mm ($0.6\lambda_0$);

low enough to avoid grating lobes but big enough to fit the curved SIW stub and the space of two patches (to avoid coupling on the neighbour SIW).

- Square copper patch side length of 2.85 mm to resonate at 30 GHz. It has been modeled as a 2D patch since it doesn't affect results significatively and reduces simulation time.

- Rogers RT/duroid 5880 patch dielectric with $\epsilon_r = 2.2$ and thickness of 0.508 mm.

- Ground plane between the patch layer and the SIW layer with a slot in order to achieve coupling between layers. The coupling slot dimensions are $1.7mm \times 0.4mm$. The slot is not centered below the patch, but instead placed with an offset of 0.875 mm from the center. This was necessary in order to fit the matching stub without intruding on neighbour unit cells.

- Rogers TMM6 SIW dielectric with $\epsilon_r = 6$ and thickness of 0.305 mm.

- Cylinders for the 'walls' of the SIW are modeled as PEC material. Their diameter is 0.4 mm, the spacing between consecutive cylinders is 0.6 mm (measured from the central axis of one cylinder to the next). The SIW is 3 mm wide.

- The matching stub length (measured from the center of the coupling slot to the central axis of the SIW wall cylinders) is 2.575 mm. Positioned 0.84 mm away from the propagation direction wall and 1.04 mm away from the side wall.

- Diameter of the 'matching pins' is 0.6 mm, and are placed 0.84 mm away from the propagating direction SIW wall and 1.04 mm away from the side wall.

- The results shown are measured assuming normal incidence on the patch. Simulations with other incidence angles has been conducted with similar results.

The process followed to determine the physical parameters of the reflectarray presented above is explained in section 3.4.

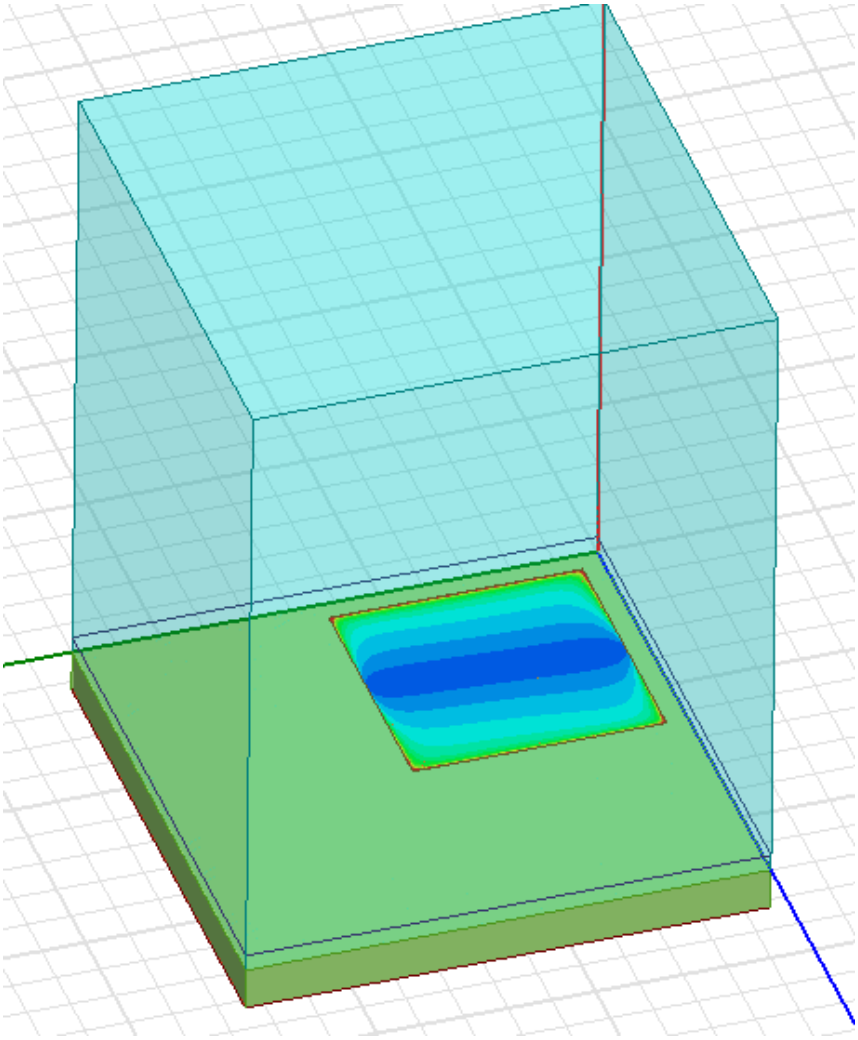

Figure 3.3: Design to find the resonating length of the patch at 30 GHz using PBC. It doesn't need to be centered because we are using PBC instead of PECPMC boundary conditions.

3.4 Simulation and results

After choosing the dielectric materials, frequency and cell size of the reflectarray, the first step in order to design the unit cell is to find the dimensions at which the square patch resonates at 30 GHz. The simulated design is shown in 3.3. It consists of a single patch antenna in reflection. It is formed by a microstrip patch on a Rogers RT/duroid 5880 substrate backed by a ground plane.

Figure 3.5 shows the reflection phase response (S_{11} curve) obtained by varying the square patch size. The reflection phase shift shown is the phase shift right above the reflectarray element after deembeding the port. Based on the dielectric constant and thickness of the substrate, it can be easily demonstrated that the

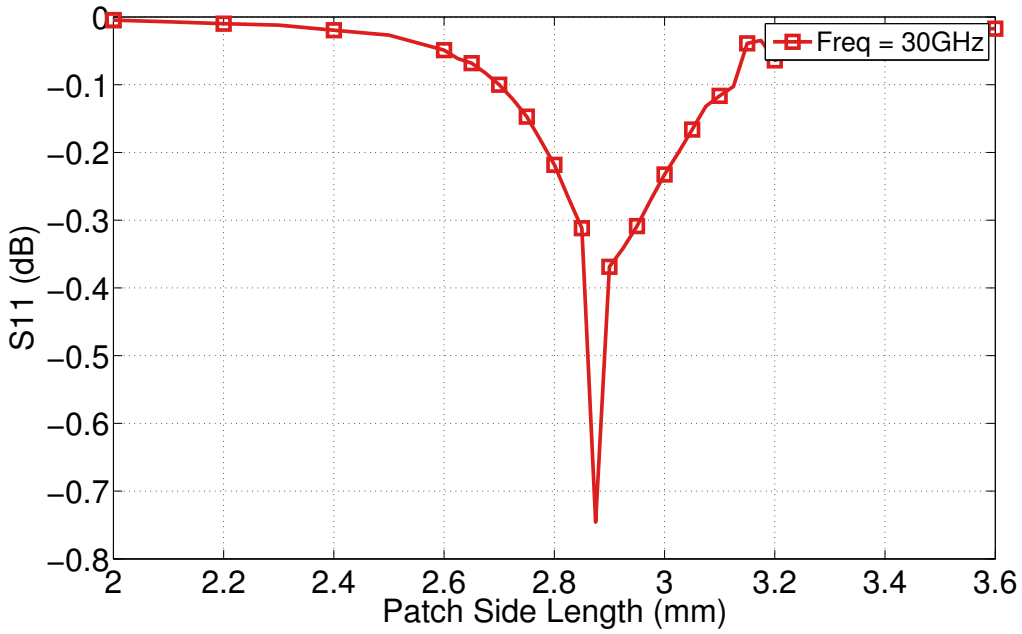

Figure 3.4: |S11| parameter of the resonant patch for different dimensions. |S11| parameter falls slightly at resonating dimensions of the patch due to conductor and dielectric losses.

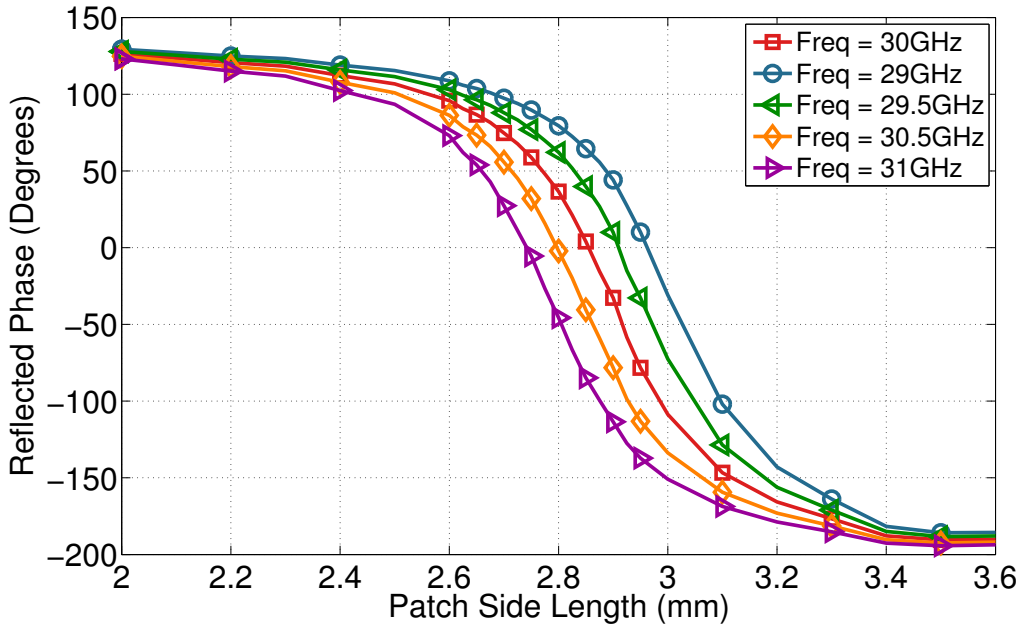

Figure 3.5: Phase of the reflected wave measured just above the patch is highly sensitive to variations both in frequency and patch size.

element resonant length is 2.85 mm. This is slightly below the theoretical expected value of $\lambda/2$, which would be 3.36 mm. This discrepancy is due to the edge effect of the fields in microstrip technologies, causing the effective electrical length of the patch to increase.

From figures 3.4 and 3.5 it can be seen that this length corresponds both to the 0° reflection phase on the phase curve as well as the minimum value for |S11|. This will be the sides length of the resonant square patch of the unit cell. This patch will remain the same in every cell of the reflectarray.

Figure 3.5 shows how the resonant dimensions of the patch changes when frequency varies. This narrow frequency band of the radiating elements is one of the reasons of the limited bandwidth of reflectarray antennas, as explained in chapter 2. We can also see the phase variation is non linear and is highly sensitive to variations both in frequency and patch size.

By using aperture coupled unit cells structure shown in figure 3.2, every patch in the reflectarray will have the same dimensions and, as a result, variations on the frequency of the impinging wave will have the same effect on every patch and thus much less effect on the full structure (at least in the patch layer of the unit cell).

Next the phase delay stub is to be added. In order to couple the electromagnetic fields on the patch with the SIW stub a slot is used. It is necessary that the stub and the patch are well coupled for the complete design to achieve a good matching. If this was not the case, the phase response of the cell would not be linear or easily predictable. If this were to happen, the objective of this design, which is to control

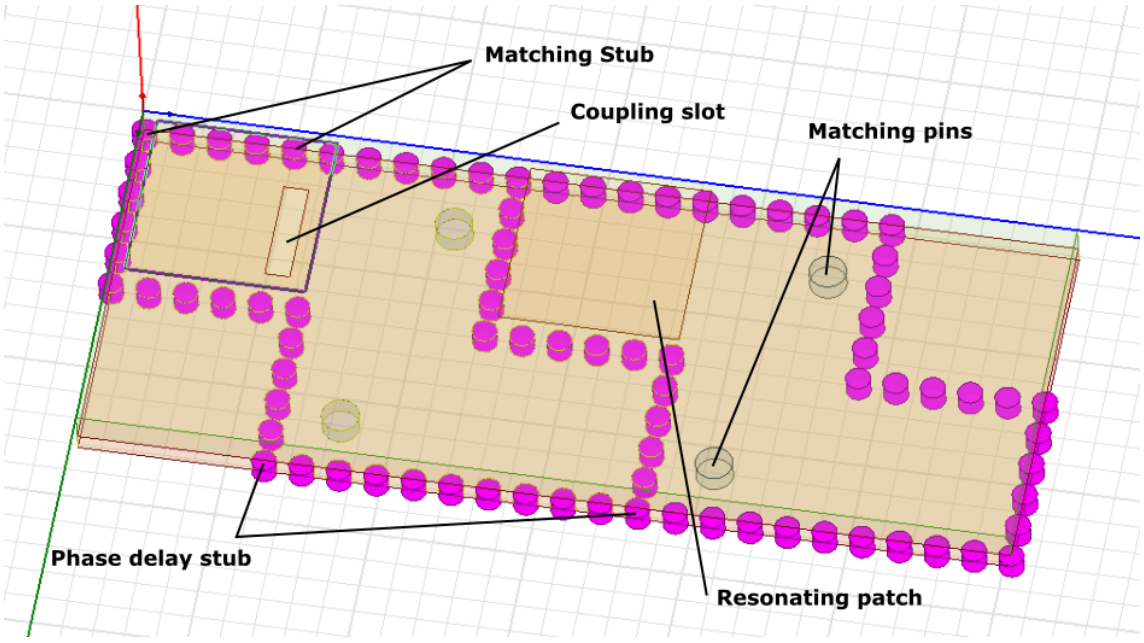

Figure 3.6: The phase delay stubs are shaped in order to maximize their length and, as a result, increase the maximum phase delay of each unit cell.

the phase delay of the unit cell by adjusting the stub length, would not be met.

In order to optimize the design we try to maximize the volume of dielectric that can be occupied by SIW within the unit cell when designing the phase delay stub. For this purpose we use the shape of the SIW stubs is illustrated in figure 3.6. Using this curved structure, we occupy the majority of the dielectric and thus achieve as much phase delay as possible, which will increase de bandwidth of the reflectarray as explained in section 2.4 of this project.

To obtain a good matching, the rectangular aperture is modified until the desired input resistance is achieved, and finally the fixed matching stub is used to compensate for the imaginary part of the input impedance. The length of this stub is, approximately, that of half of the guided wavelength. The matching stub is shown in figure 3.6. The guided wavelengths on a rectangular waveguide is obtained through

$$\lambda_g = \frac{2\pi}{\beta} \tag{3.1}$$

with β being the phase constant of the propagating mode of the waveguide, which is

$$\beta = \sqrt{k^2 - k_c^2} \tag{3.2}$$

with

$$k_c = \sqrt{\left(\frac{m\pi}{a}\right) + \left(\frac{n\pi}{b}\right)} \tag{3.3}$$

being k_c the cutoff wave number of the TE_{mn} mode propagating on a rectangular waveguide (RWG) of width **a** and height **b** [17]. We also have to take into account the use of SIW instead of normal waveguides. In SIW structures there is no clear value for the ***a*** dimensions since the sides of the waveguide are made with via holes. We can find different approximations for this value depending on the diameter of the via holes, the spacing between them and other dimensional parameters. The approximation used, as well as others, can be found at [16]. The one we employ here is

$$a_{eff} = a - 1.08\frac{d^2}{s} + 0.1\frac{d^2}{w} \tag{3.4}$$

being a_{eff} the width of a rectangular waveguide with the same propagation characteristics; ***d*** is the diameter of the metal vias, **a** represents their transverse spacing and **s** is their longitudinal spacing.

Combining equations (3.1), (3.2), (3.3) and taking into account that $a = w_{eff}$ and the mode propagating will be TE_{10}, we arrive at

$$\lambda_g = \frac{2\pi}{\sqrt{k^2 - \left(\frac{\pi}{a_{eff}}\right)}} \tag{3.5}$$

and finally, the length of the matching stub will be approximately

$$L_{stub} = \frac{\lambda_g}{2} \tag{3.6}$$

Still, this is only an approximation. The dimensions of this stub, as well as others such as the slot dimensions or the patch position must be adjusted by using full wave simulation software, in our case, HFSS.

In order to adjust the different dimensions using HFSS, the structure is fed from below the patch by injecting a wave on the SIW and checking the S_{11} parameter (only S parameter as it is a one-port network). To achieve a good matching in this situation the absolute value of the S_{11} parameter should be minimized at the operating frequency. This is equivalent to maximizing the energy coupled from the SIW through the slot to the patch antenna and radiated towards free-space. We consider values of $|S_{11}|$ under -25 dB at the operating frequency as good matching. If we achieve a good matching this way, the system will be well matched when operating as a reradiating element due to reciprocity. Figures 3.7 and 3.8 show the input impedance (Z_{in}) and $|S_{11}|$ parameters respectively. We can see in figure 3.7 that $Re[Z_{in}] \simeq 50\Omega$ and the $Im[Z_{in}] \simeq 0\Omega$ at the operating frequency, which is sign of a good matching at microwaves for our network. Figure 3.8 shows that the $|S_{11}|$ parameter under the described circumstances is below -25 dB at the design frequency, 30 GHz. Figure 3.8 also indicates that the matching worsens faster for higher frequencies than it does for frequencies lower than 30 GHz.

The shape of the SIW phase delay stub made necessary the use of matching pins, similar to tunning screws in usual waveguides, in both turns of the waveguide. These matching pins can be seen in figure 3.2. The position, as well as the diameter of these pins were optimized again by using parametric HFSS simulations with the objective to achieve as good of a matching as possible in the structure.

In a second step, the input side of the SIW (previously used as a port for the matching) is loaded with a short circuit. The reflection coefficient of the incident

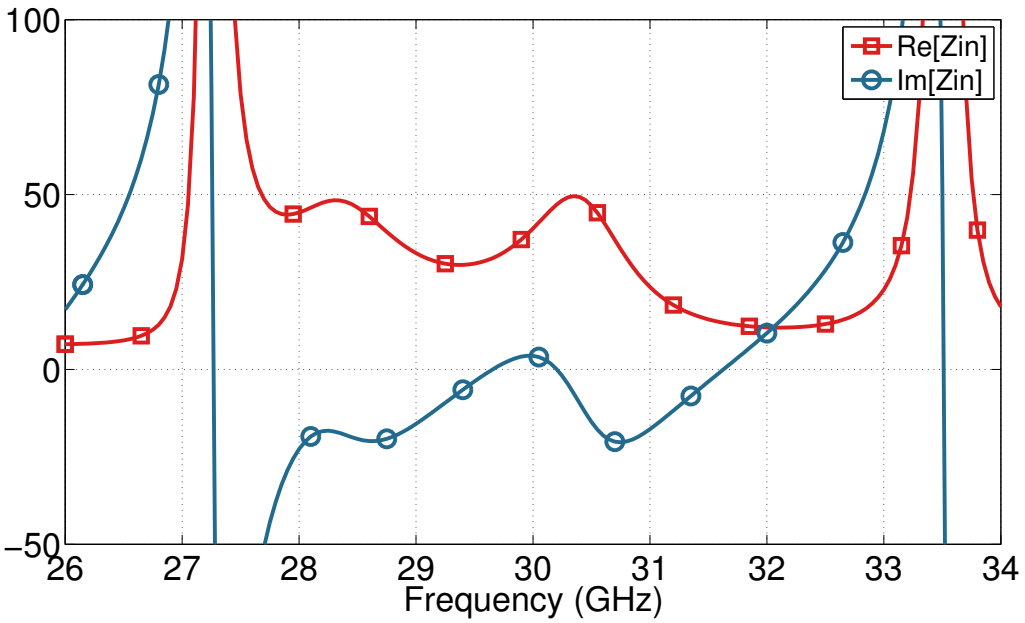

Figure 3.7: Z_{in} of the unit cell fed as an active radiating element is close to 50Ω at design frequency (30 GHz).

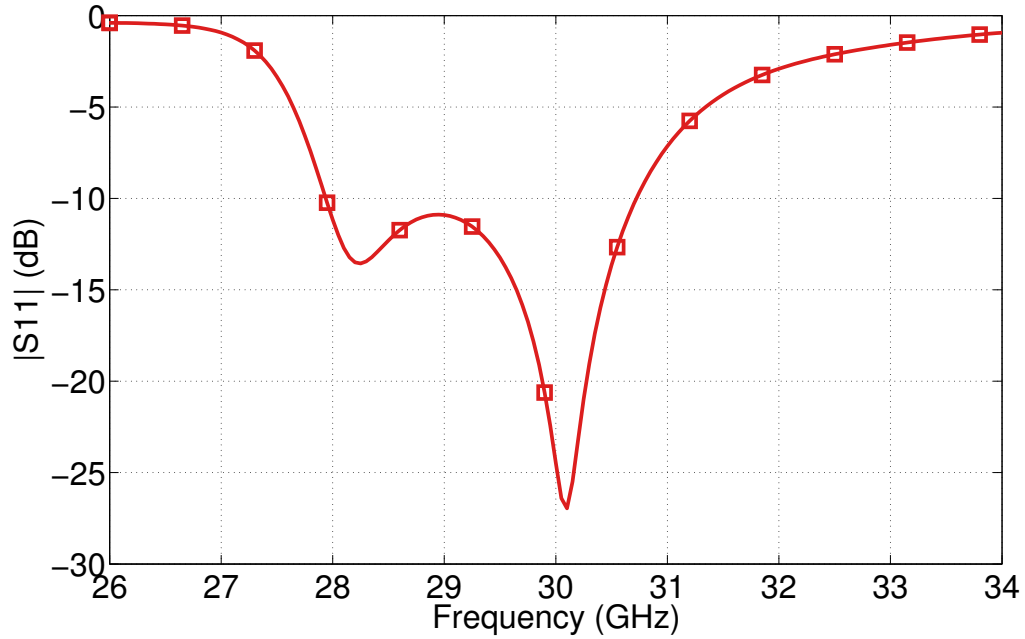

Figure 3.8: $|S_{11}|$ parameter of the unit cell fed as an active radiating element. It achieves a minimum at design frequency (30 GHz).

plane wave is computed for different lengths of the SIW, assuming again local periodicity (PBCs) and taking into account the mutual coupling between elements. In order to measure the phase for all the possible lengths of the SIW stub, several parametric simulations were needed, since the shape of the stubs require to 'move'

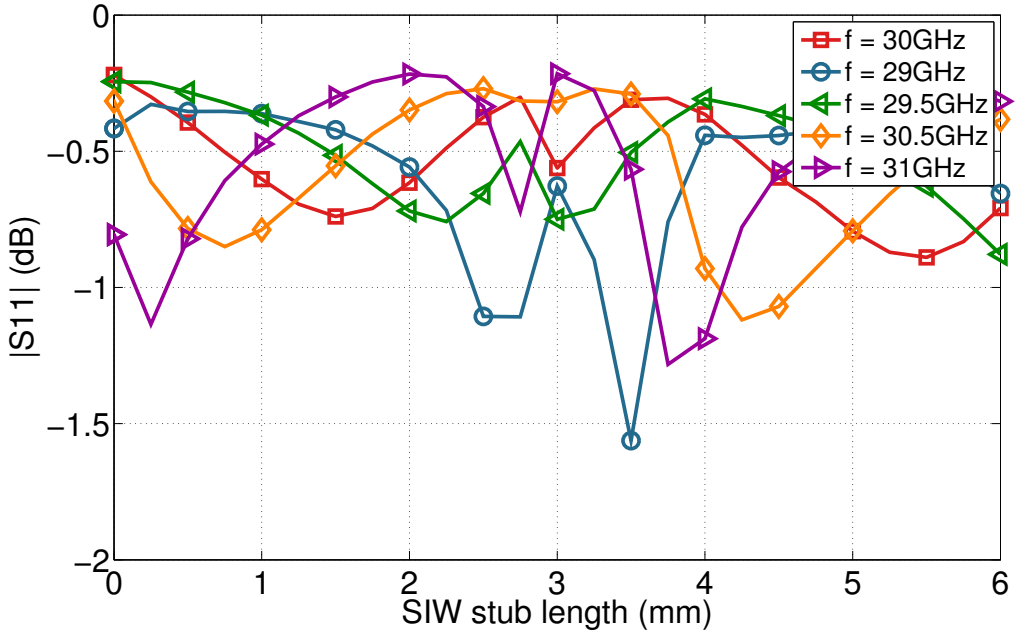

Figure 3.9: $|S_{11}|$ is above -1 dB for most stub lengths when operating near the design frequency. This represents the gain at the structure when functioning as a passive radiating element.

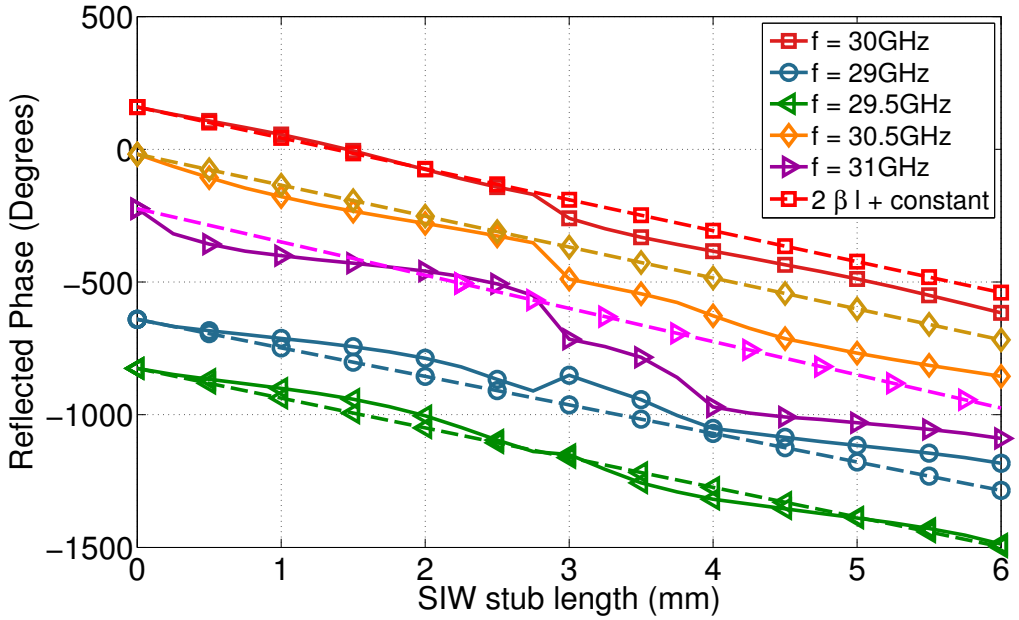

Figure 3.10: Phase delay is linear and similar to that of a theoretical waveguide of the SIW stub dimensions when operating on the design frequency. Solid lines represent the simulated value for the structure; dashed lines represent the theoretical phase delay of a RWG of the same dimensions. Phase becomes less linear as we move away from the design frequency. A significant variation occurs at 3 mm length.

different walls each time, as well as remove adaptation cylinders when they are no longer needed.

Figure 3.9 shows the computed amplitude for the reflection coefficient for different SIW stub lengths. We see that the reflection losses increase slightly ($|S_{11}|$ value decreases) the longer the SIW stub is. More importantly, the losses are higher the farther we are from the design frequency (30 GHz), but is kept above 1 dB in most of the situations, which are considered acceptable losses.

Figure 3.10 shows the phase delay introduced by the structure for different stub lengths and frequencies. It can be seen that, at the operating frequency, the phase is linear and very similar to the theoretical phase-shift of a rectangular waveguide of the same dimensions and dielectric (assuming a equivalent RWG for the SIW structure based on (3.4). The phase-shift undergoes a significant change at the length of 3 mm at all frequencies. This is to be expected as at that length we are changing the dimensions of the curve of the SIW stub, and the phase shift is harder to predict with the theoretical phase constant on de RWG. The phase-shift introduced is still fairly linear and easy to predict.

This result is really good considering the curved shape of the stub. The phase-shift of the element becomes gradually less linear (and similar to the theoretical

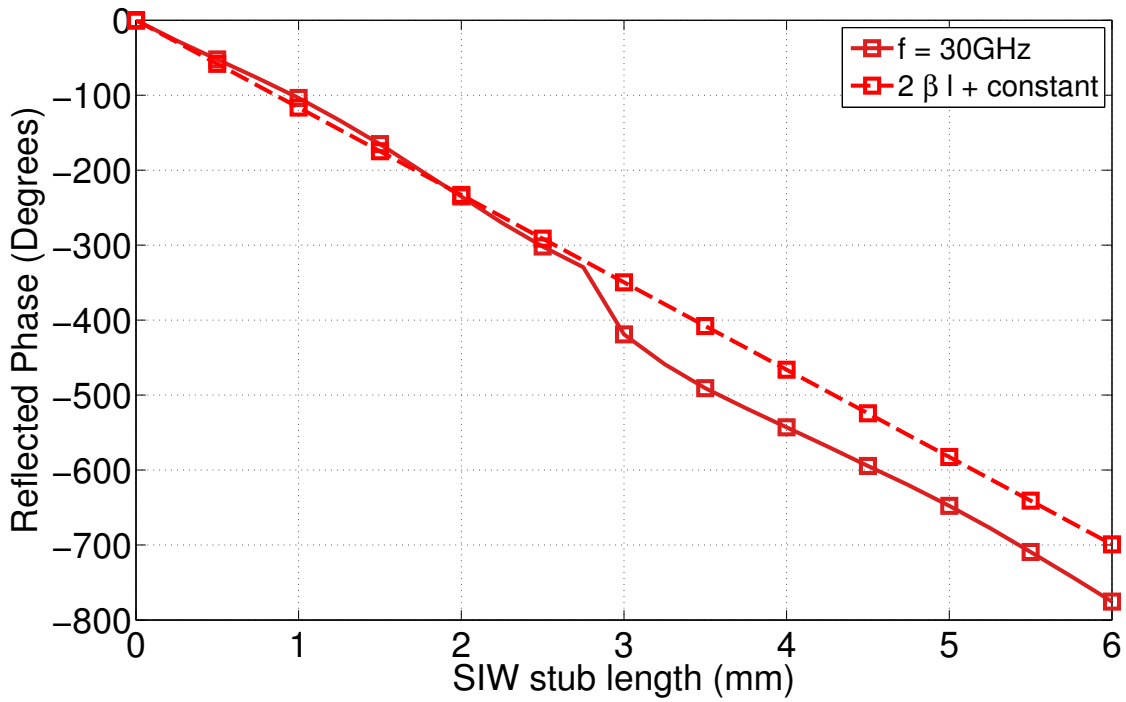

Figure 3.11: Phase shift introduced by the structure at the operating frequency is fairly linear and similar to the theoretical value of the phase-shift on a RWG of the same dimensions. Phase shift range is close to 800°.

RWG value) as we move away from the operating frequency. This is expected, as the electrical length of the stub will vary and, more importantly, the matching between patch and SIW worsens as the frequency changes (As shown in **??**).

Figure 3.11 shows the normalized phase-shift of the element for different SIW stub lengths at the design frequency. It can be seen that we achieve a phase-shift range of almost 800° while using a small enough cell size to avoid grating lobes and with a passive planar structure. This is due to the shape of the SIW stub, which uses most of the dielectric surface available to increase the phase-shift of the element. This phase shift could be increased farther by choosing denser dielectric material for the SIW layer or by stacking an additional SIW layer.

With this linear phase behaviour we can easily adjust the SIW stub to the necessary length to achieve the phase delay required for each unit cell of the reflectarray surface. As a result, this structure can be used for every reflectarray element of any reflectarray design by slightly varying the position of the SIW walls while taking advantage of the benefits of using the TTD technique and SIW technology over the classical microstrip designs.

In conclusion, the phase shift element design in this chapter is functional, low cost and usable for the design of real reflectarray structures. By using SIW instead of microstrip to implement the phase-delay stub we achieve lower losses and require one less dielectric layer, which make SIW designs much cheaper and faster to fabricate.

Chapter 4

Rectangular Waveguide-Infinite Array Simulator

4.1 RWG-IAS on reflectarray design

4.1.1 Introduction

As explained in section 2.3, analysis techniques to calculate mutual coupling between all the different elements of a reflectarray are to costly and as a result, PBC are commonly used as an approximation when designing reflectarray structures. When measuring reflectarray unit cells in laboratory conditions we come across the same problem: the only way to measure in its real array environment (that is, taking into account the coupling with the rest of the radiating elements in the structure) is to build the complete reflectarray. This is especially inconvenient since new reflectarrays would have to be built and measured whenever the model is updated.

In the case of measurements, PBCs can obviously not be artificially fabricated. An easy approach is to use the usual rectangular waveguide (RWG) for the measurement. A RWG can be used to simulate the behavior of an array element in an infinite array in an exact way, under some conditions, as it was shown in [18]. This approach is referred to as the rectangular waveguide infinite array simulator (RWG-IAS).

4.1.2 RWG-IAS description and theory

The RWG-IAS was first introduced in [18]. A complete demonstration of the RWG-IAS principle and required assumptions can be found at [7]. In this project we limit ourselves to present the RWG-IAS functionality for measuring reflectarray unit cells, as well as present the fundamental expressions that model its functionality.

RWG-IAS consists on loading a RWG with the unit an specific amount of unit cell elements from de reflectarray design. The structure simulated is an infinite rectangular lattice, where the elements are repeated by symmetry (not by translation). A load placed in the RWG and excited by the TE_{10} mode exactly models the incidence of two plane waves as described above on an infinite array of such loads, periodically repeated by symmetry around both array axes, as shown in figure 4.1.

It is important to note that the incidence angle on the load of the RWG-IAS structure θ can by obtained from:

$$|\sin\theta| = \frac{\pi}{k_0 a} = \frac{c_0}{f_0 a} \tag{4.1}$$

and the total field on any point of the WG:

$$\vec{E}_{tot} = 2E_y \cos\left(\frac{\pi x}{a}\right) e^{\left(-j\sqrt{k_0^2 - \left(\frac{\pi}{a}^2\right)}z\right)} \hat{e}_y \tag{4.2}$$

Our aim is to use the RWG to simulate an infinite array of the same radiating element in order to be able to measure the unit cell of the designed RA on an array environment, obtained by translation of this element. However, we showed that the RWG actually simulates an infinite array of elements, but where the infinite lattice is obtained by symmetry of the element with regard to the RWG lateral walls, such as illustrated in 4.1. As a result, the RWG-IAS can be employed to simulate the 'translation array' only in the particular case where both symmetry and translation arrangements are the same. This is only possible if the two following conditions are met:

First, the element must by symmetrical around both axis of the transversal plane of the RWG. The RWG height b must be a multiple of the array lattice half spacing in the y dimension dy (E field direction) in order to exactly fit a natural number of half elements.

$$b = \left(\frac{p}{2}\right) d_y \quad with \quad p \in \mathbb{N}^* \tag{4.3}$$

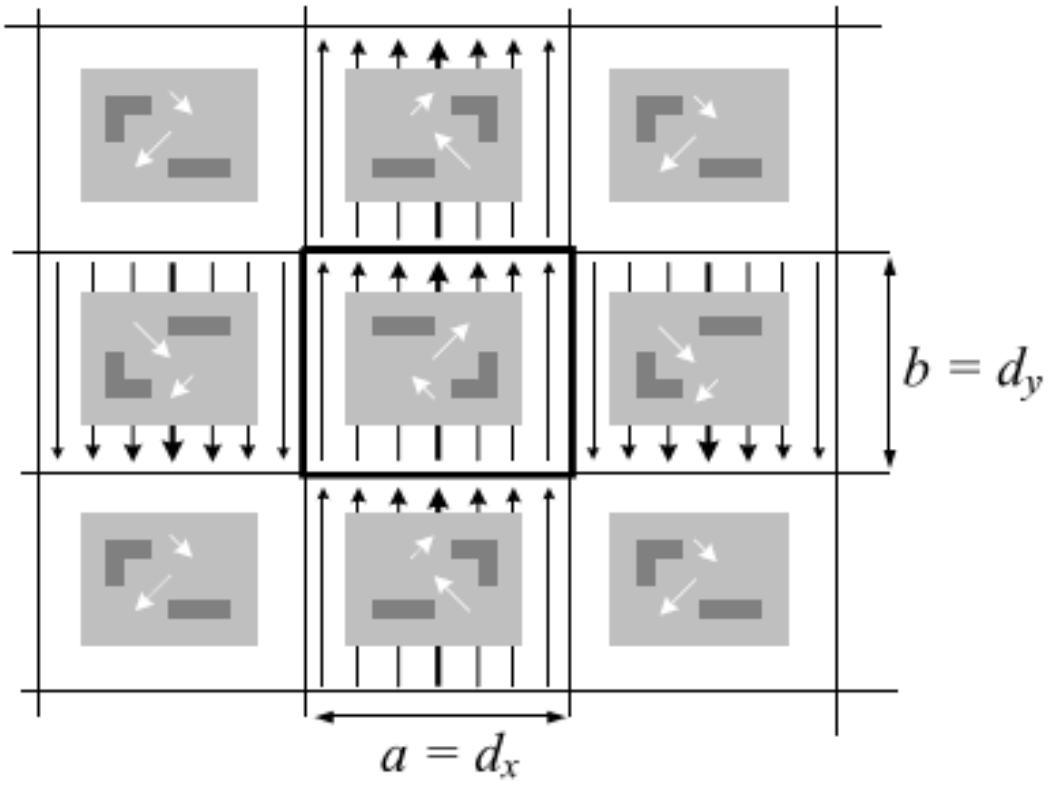

Figure 4.1: The load of a RWG-IAS is repeated by symmetry, not by translation, in both axis directions. Reproduced from [7].

and the RWG width a must be related to the array lattice spacing in the x dimension d by:

$$a = \left(\frac{m}{2}\right) d_x \quad with \quad m \in \mathbb{N}^* \tag{4.4}$$

where m is the number of 'half-elements' placed in the RWG in the x dimensions. Figure 4.2 illustrates how the same array can be simulated by two different RWG dimensions, both satisfying (4.4)

4.1.3 Grating lobes on RWG-IAS

In this section, we link the RWG-IAS structure to the issue of grating lobes referred to in section 2.2 of this project. Let us remember the condition on the regular reflectarray of element spacing **d** and main beam direction (or incidence angle, whichever

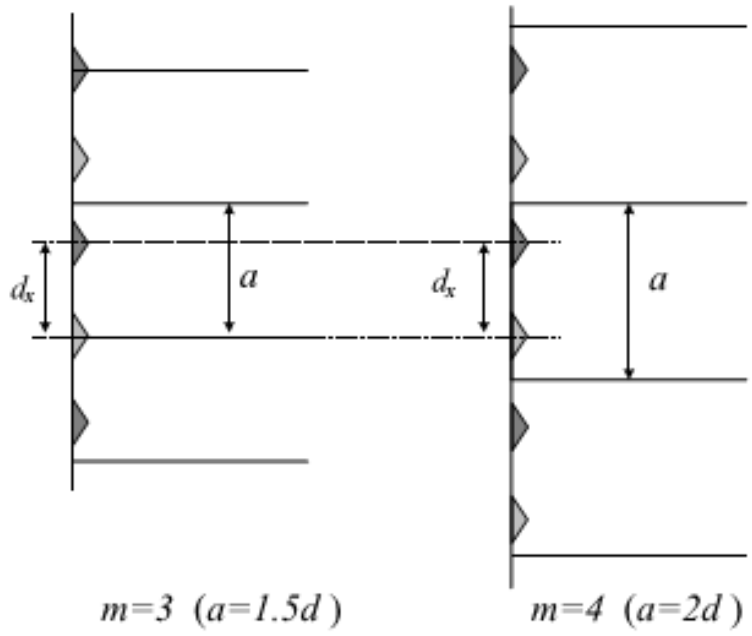

Figure 4.2: Two RWG-IAS arrangements loaded with the same unit cells but using different waveguide dimensions. Reproduced from [7].

is larger) θ so that no grating lobe occurs:

$$\frac{d_x}{\lambda_0} < \frac{1}{1 + |\sin\theta|} \tag{4.5}$$

Also, by substituting equation (4.4) in (4.1), the following relation between frequency and angle of incidence θ when using a RWG-IAS structure (written as a function of RWG-IAS parameters $\mathbf{m}$ and d_x by substituting (4.4) in (4.1)) we find:

$$\sin\theta = \frac{\lambda_0}{m d_x} \tag{4.6}$$

Now, by introducing (4.6) in (4.5), we arrive at the new condition (4.7).

$$\frac{d_x}{\lambda_0} = \frac{1}{1 + \frac{\lambda_0}{m d_x}} \tag{4.7}$$

This expression can be rearranged rewritten in terms of frequency rather than wavelength as seen in (4.8) to manage better understanding of the meaning of this condition. The limit frequency where the first grating lobe appears is referred to as f_{GL}.

$$f < f_{GL} = \frac{c_0}{d_x}\frac{m-1}{m} \tag{4.8}$$

In (4.8) we manage to rewrite the no gratin lobes condition by using geometrical parameters of the RWG-IAS structure. We will now introduce in this expression the

cutoff frequency f_{10} of the dominant mode propagating along the RWG-IAS, which is first rewritten using (4.4) as:

$$f_{10} = \frac{c_0}{2a} = \frac{c_0}{md_x} \tag{4.9}$$

which finally yields the condition on the frequency so that the array simulated by the RWG-IAS exhibits no grating lobe (merging (4.9) and (4.8)):

$$f < f_{GL} = (m-1)f_{10} \tag{4.10}$$

Equation (4.10) provides a relation between the frequency at which grating lobes appear for a given structure, the **m** of the RWG-IAS structure and the cutoff frequency for the fundamental mode of the RWG used in the said RWG-IAS design.

For RWGs with $a > 2b$, where a and b are the dimensions of the RWG, the second mode is the TE_{20}, so the frequency band where the only fundamental TE_{10} mode propagates is:

$$f_{10} < f < f_{20} = 2f_{10} \tag{4.11}$$

If we unify these two conditions, we find the band where the RWG-IAS can be employed in its fundamental mode to simulate an array without grating lobes is:

$$f_{10} < f < min[2f_{10}, (m-1)f_{10}] \tag{4.12}$$

Now, let us study the band as a function of the parameter **m**, which is the number of half-elements placed in the RWG-IAS, defined in (4.4):

- For half a cell or a single cell embedded in the RWG-IAS (m = 1 and m = 2, respectively), there is no frequency where the first mode of the RWG propagates for a RA without GL.

- For m = 3, which means that 1.5 cell are placed inside the RWG-IAS, the first grating lobe appears at the same frequency as the 2nd mode of the RWG, so the whole band can be used.

- For m > 3, the limiting factor for the upper band of the frequency range measured is the appearance of the 2nd mode of the RWG, so we always have in this case $f_{10} < f < f_{20} = 2f_{10}$

A conventional RWG with a > 2b operated in its fundamental TE_{10} mode can be used to simulate the reflection of a plane wave of incident angle θ on an infinite array of symmetrical elements and constant unit cell spacing **d**. By substituting according to (4.4) in (4.1) we can write:

$$|\sin\theta| = \frac{\lambda_0}{md} = \frac{c_0}{mdf} \tag{4.13}$$

where the width of the RWG **a** is linked to **d** by equation (4.4). As mentioned before, in order to simulate an infinite array without grating lobes, it is necessary to choose $m \geq 3$. This means, for a RWG-IAS with a > 2b, that the band available for monomodal measurement corresponding to an array free of grating lobes is:

$$f_{10} < f < 2f_{10} \quad with \quad f_{10} = \frac{c_0}{m\ d} \tag{4.14}$$

So, for a given array element spacing **d**, the only free parameter is**m**, which is twice the number of array elements placed in the RWG-IAS. As mentioned, **m** must be equal to or larger than 3 for the measurement of an array without grating lobes. Also, the choice of **m** determines the relation between frequency and angle θ as seen in (4.6).

The maximum and minimum incidence θ angle that can be simulated is restricted by the limiting frequencies of the design being f_{10} and f_{20}. As a result, $\theta_{max} = \theta(f_{10}) = 90°$ and $\theta_{min} = \theta(f_{20}) = 30°$. This values can easily be obtained by simply substituting (4.9) and (4.11) on 4.13

More than one incidence angle can be tested at the same frequency if several RWG-IASs structures, each with different m values, are built. Even in this case, the frequency and incidence angle on the element cannot be freely chosen, since $m \in N$.

RWG-IAS structures loaded with reflectarray unit cells are an easy approach to empirically measure the unit cell operating on an array environment, without the need of constructing the full array. This method has some limitations that have been reviewed in this section, such as the required symmetry of the unit cell measured and the limited amount of incidence angles that can be measured.

4.2 RWG-IAS Simulation

In this section we simulate a RWG-IAS structure based on the unit cell designed earlier on this project in order to facilitate its future construction. As commented

before in this chapter, RWG-IAS structures loaded with reflectarray unit cells are used to measure the unit cell operating on an array environment, without the need of constructing the full array.

For this RWG-IAS we have used a RWG loaded with 2 complete unit cells, which is the same as to say that we used a value of $m = 4$, according to this chapter nomenclature. By doing so we make sure we can measure the unit cell with only the fundamental mode propagating on the waveguide and, as explained earlier in this chapter, without the risk of appearance of grating lobes in the final array structure. Figure 4.3 shows the structure of the RWG-IAS structure simulated.

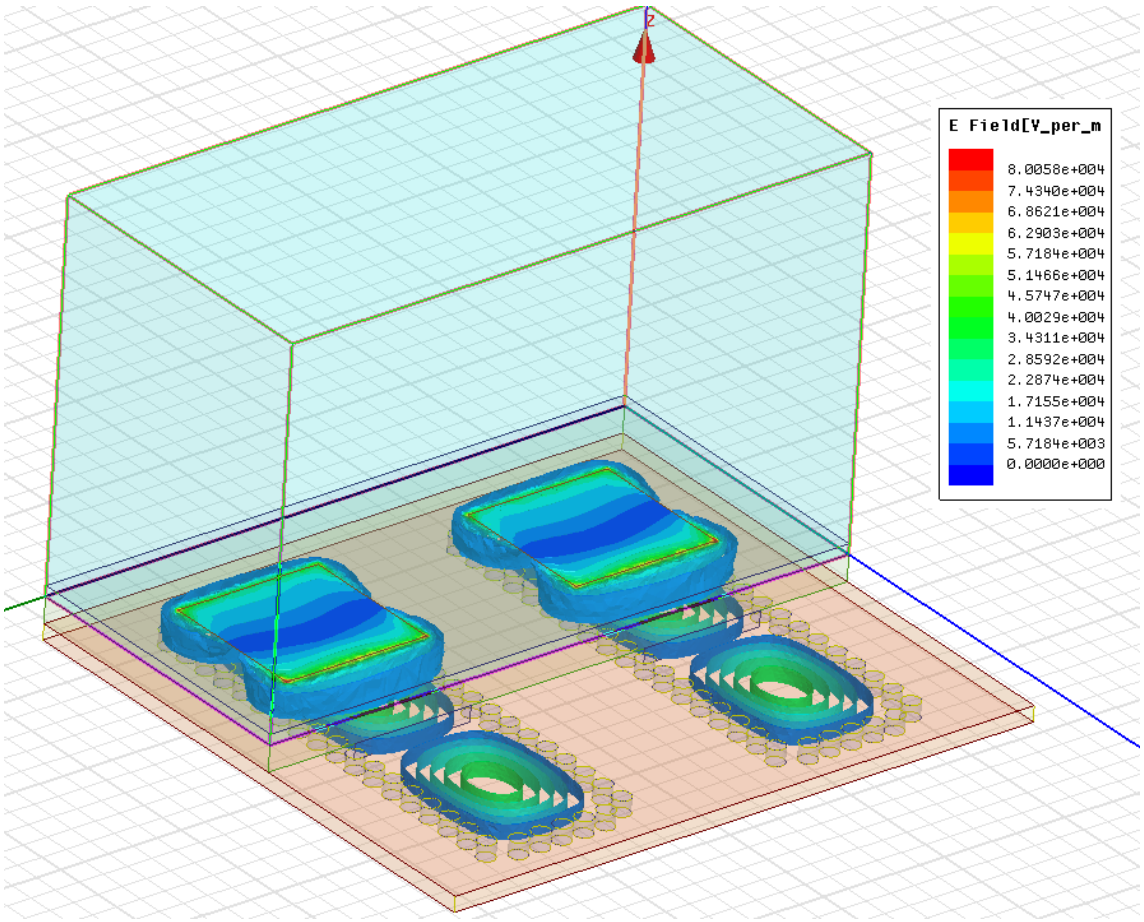

Figure 4.3: RWG-IAS structure for the measurement of the unit cell proposed on chapter 3. Two full phase-shift unit cells are loaded on a RWG.

The structure of the unit cells is similar to that of the chapter 3 of this project. It is not the exact same because of the need to satisfy the symmetry requirements of the RWG-IAS. As a result, the resonant patches are centered in their respective unit cells. For simplicity's sake, the SIW structure is straight, with no bents, as good

adaptation for that structure has already been proven possible on chapter 2 and there is no need to repeat the process. The dimension of the RWG is two element spacing wide and 1 element spacing high ($a = 12mm$ and $b = 6mm$).

The main objective of this design is to verify the RWG-IAS structure for a future laboratory test of a unit cell prototype. The result of the following simulations don't validate the cells themselves, but allow us to ascertain that the unit cell behaviour when simulated with ideal PBC conditions is the same as that of the unit cell when simulated in the RWG-IAS structure. This way we can be sure that the design is solid and the future prototype testing will yield valid results, however good or bad they might be. With the characteristics of the design, and making us of (4.1) it is immediate to calculate that the unit cell will be measured with an incidence angle on $\theta = 56.44°$

Same as last chapter, the first step is to make sure that the coupling between the patches and SIWs are well matched. To do so we feed the structure from below, same as if it was an active radiating patch fed by the SIW through the slot. Figures 4.4 and 4.5 show the $|S_{33}|$ parameter, as well as the active S12 and S11 parameters. Port 1 and 2 are the SIW ports and port 3 is the RWG port. $|S_{33}|$ parameter allows us to see if the power coming through the RWG is properly transmitted through the resonating patches and the SIW. Active $|S_{21}|$ and $|S_{11}|$ parameters indicate the amount of power coupled between both patches and the power not transmitted from the SIW to the patch when both ports are active at the same time.

Figure 4.4 shows $|S_{33}|$ parameter. We can see it spikes down (to about -25 dB) at the operating frequency, which indicates the power is being transmitted to the SIW correctly. Figure 4.5 shows active $|S_{11}|$ and $|S_{21}|$ parameters. At the operating frequency they also achieve a minimum (below -25 dB), indicating that very little to no power is reflected at the slot back to the SIW or coupled to the other patch, when both ports are active simultaneously. We can conclude that the overall design is well matched.

Next is to measure the phase shift of the unit cells for different SIW stub lengths. Following the steps of chapter 3, we load both ports 1 and 2 (the SIW ports) with a short circuit implemented as a SIW wall. With only port 3 (the RWG port) active we measure the phase shift introduced by the unit cells directly. Port 3 is deembed so that it measures the phase shift directly above the resonant copper patch, same

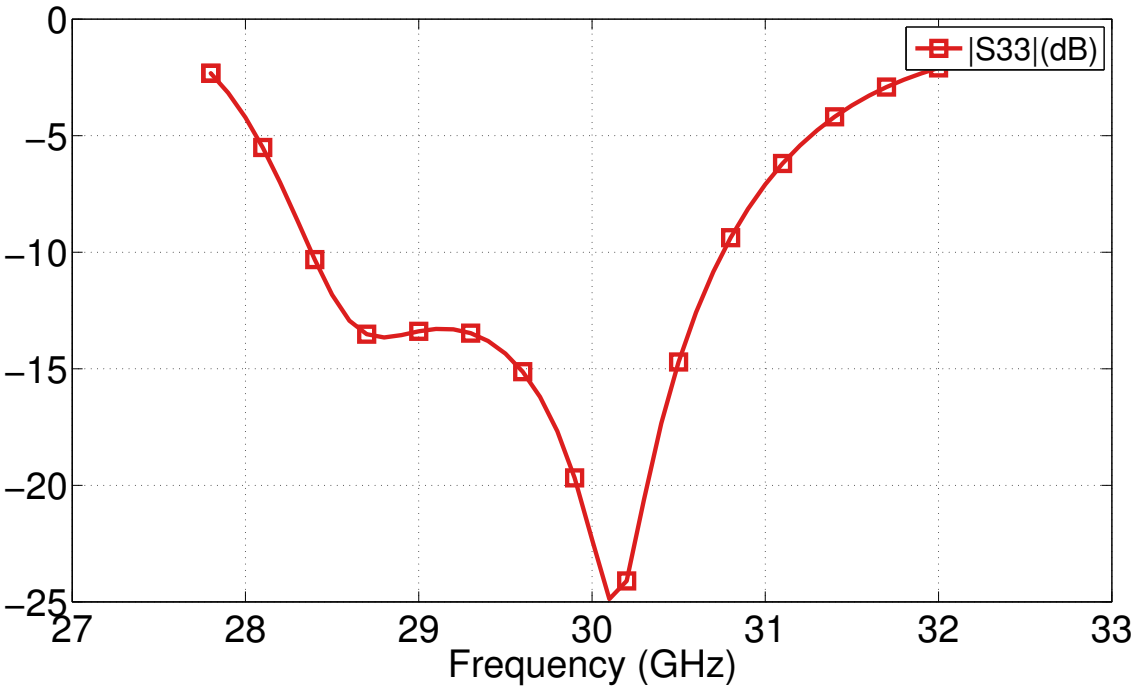

Figure 4.4: $|S_{33}|$ parameter shows a good matching at the design frequency, most power is transmitted from port 3 to the rest of the ports through the resonant patch to the SIW through the slot.

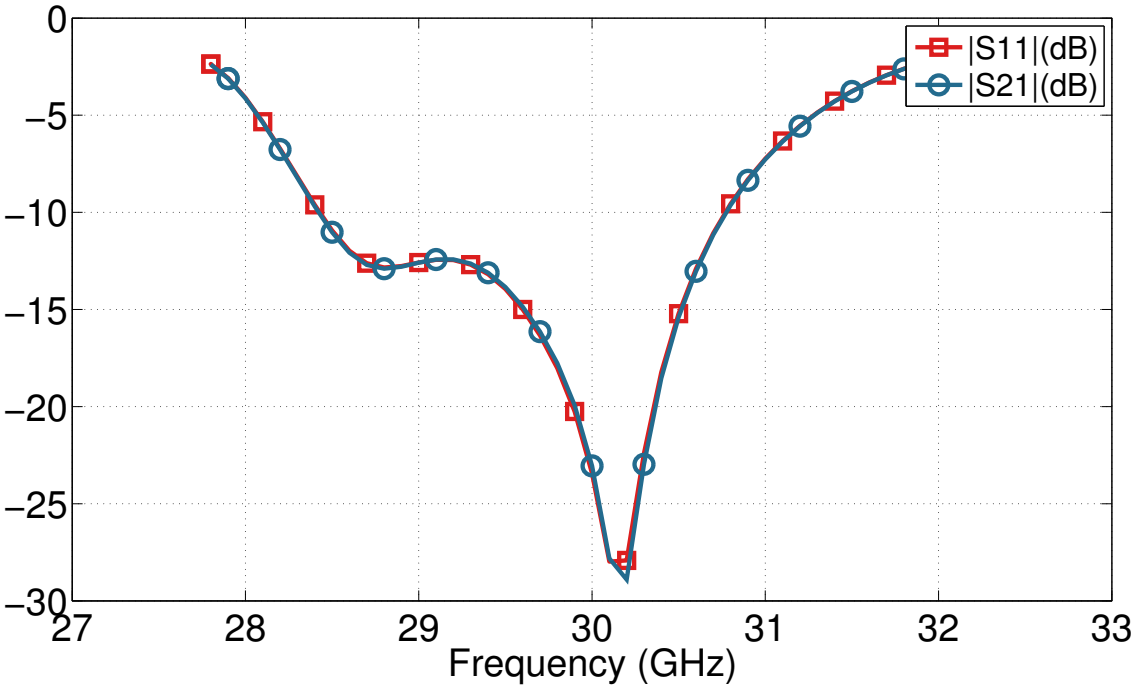

Figure 4.5: Low $|S_{11}|$ and $|S_{21}|$ indicates no unwanted reflection at the slot nor coupling between ports 1 and 2 at the design frequency.

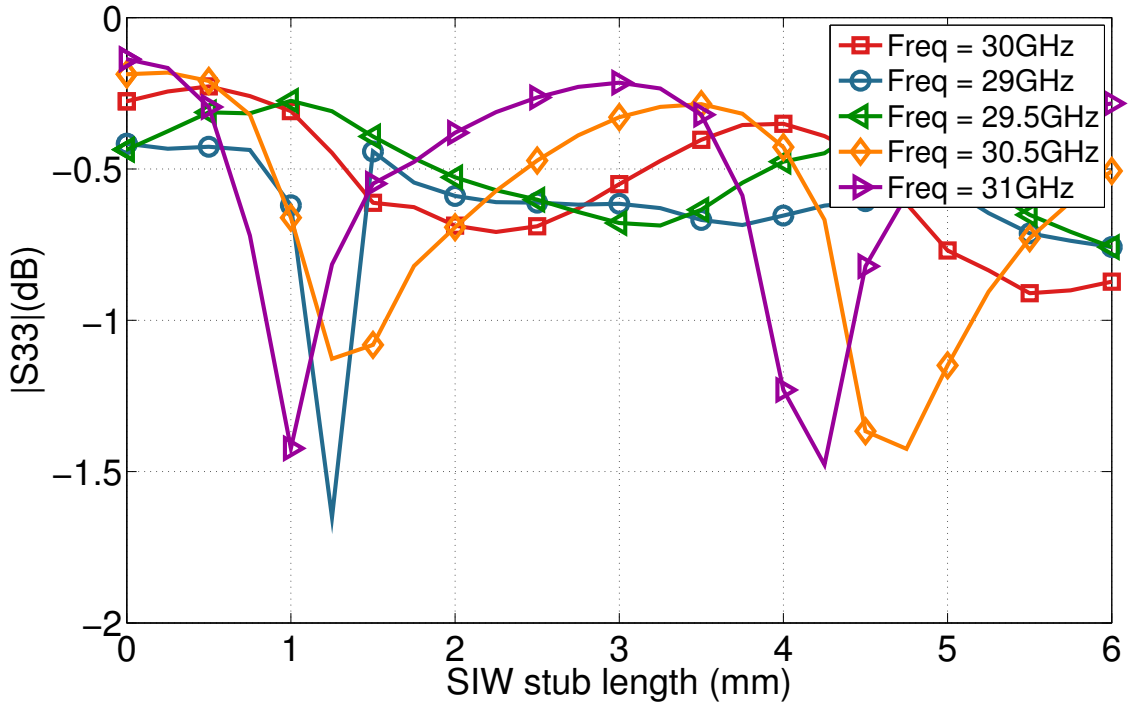

Figure 4.6: $|S_{33}|$ is above -1 dB for most stub lengths when operating near the design frequency. This represents the gain at the structure when functioning as a passive radiating element.

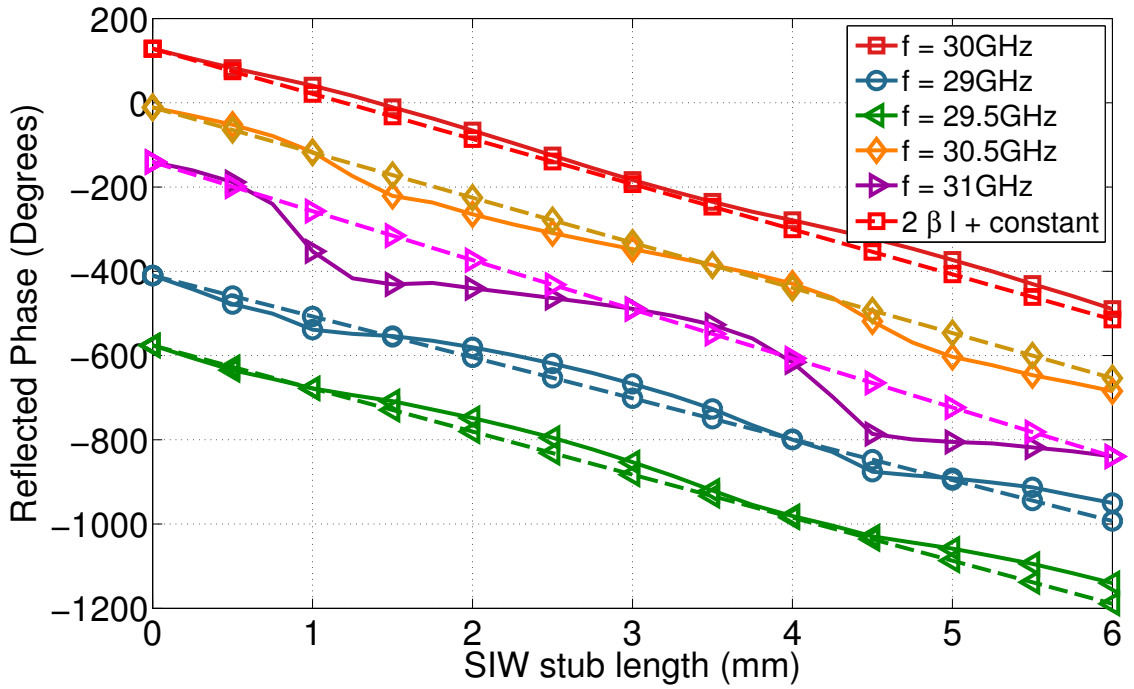

Figure 4.7: Phase delay is linear and similar to that of a theoretical waveguide of the SIW stub dimensions when operating on the design frequency. Solid lines represent the simulated value for the structure; dashed lines represent the theoretical phase delay of a RWG of the same dimensions. Phase becomes less linear as we move away from the design frequency.

as in the design of chapter 3.

Figure 4.6 shows the $|S_{33}|$ parameter. This time, this parameter represents the loses of the unit cell when functioning as a passive radiating element. The higher this value, the less loses the unit cell introduces. We see it decreases the longer the SIW stub is, but is kept above 1 dB at the operating frequency. The loses are higher ($|S_{33}|$ is lower) the farther we are from the design frequency (30 GHz).

Figure 4.7 shows the phase shift introduced by the design $[\angle(S_{33})]$ for different SIW stub lengths, and compares it to the theoretical phase shift of a waveguide of the same characteristics as the SIW used. It can be seen that the phase is almost perfectly linear on the operating frequency, and degrades more as the frequency is farther from 30 GHz. The resultant phase shift is also similar to the theoretical phase-shift of a rectangular waveguide of the same dimensions and dielectric (assuming a equivalent RWG for the SIW structure based on 3.4). Figure 4.7 shows the phase shift range achieved with a 6 mm stub is above 600° for this design.

The unit cell placed as a load on a RWG-IAS structure functions as expected from a design with PBC, which validates the design and makes ground to the future manufacturing of a prototype for laboratory testing. This chapter has served us to ensure that a well designed RWG-IAS structure is a good method to evaluate reflectarray elements without the need of building a full reflectarray surface. The structure designed on this chapter can be directly fabricated and measured knowing the results will be valid.

Chapter 5

Conclusions and future lines of work

In this chapter, the contents and results of this project are reviewed, followed by a presentation of potential continuations of this project.

Chapter 2 served as an explanation of the state of the art of reflectarray design, namely reflectarrays based on aperture coupled patches, with the objective of setting the ground knowledge for both chapter 3 and 4. The basis of periodic boundary conditions (PBC) based on Floquet's Theorem were exposed. Also, the phase needed on each reflectarray element was computed based on equations derived from array theory and free space planar wave travelling equations. By doing so, the phase required for every element with any given feed position and main beam direction for pencil beam arrays can be easily computed. Lastly, in this chapter, true time delay (TTD) was introduced as a way to improve the bandwidth of the reflectarray antenna.

In chapter 3, the full design of a phase shift element for a reflectarray surface based on aperture coupled patches was designed and simulated using Ansoft's HFSS. The main innovation of this design was the use of SIW technology to implement the phase-delay stub, as this technology has yet to be used extendedly for this applications. Also, the geometry of the SIW stub was thought so that the stubs length is the maximum possible and thus the phase delay achievable is as high as it can be in order to increase the bandwidth of the design. By carefully choosing the right materials and dimensions, a fully functioning unit cell was designed. The phase shift was linear with the stub length and, as a result, easily predictable. The most obvious future work line emerging from this chapter is the study of the effects of adding of multiple layers of SIW coupled with slots with the aim of introducing

even more maximum phase delay. The design of the full reflectarray, computing the final radiating pattern when using the designed unit cells and different feeds is as well a possible continuation to the studies done on this chapter.

Chapter 4 tackled the explanation and design of a rectangular waveguide - infinite array simulator (RWG-IAS) as a way to measure unit cell prototypes on an array environment without the necessity of building a full reflectarray. The characteristics of this structure, as well as its limitations, were briefly exposed at the beginning of this chapter. Next, the design simulation of the RWG-IAS structure based on the phase shift element designed on chapter 3 using Ansoft's HFSS was conducted with the objective of validating the design and serve as a model for future prototypes. The results were satisfactory and we concluded that this RWG-IAS structure could be converted into a physical design in order to measure a real prototype of the unit cell designed. The obvious future line of work regarding this chapter is the manufacture of this prototype and its measure using a vector network analyser (VNA) to definitely validate the design.

The work done in this project may serve as a validation of the effectiveness of SIW technology in reflectarray element design, as well as a guidance to those seeking to design phase-shift elements for reflectarray antennas. It also serves as a union of different reflectarray design techniques that are used by different authors, but not very commonly put together.

Bibliography

[1] Eduardo Carrasco Yepez. *Nuevas teconologias y tendencias en antenas espaciales.* 2014.

[2] JA Zornoza and JA Encinar. Design of shaped beam reflectarrays for direct broadcast satellites. *JINA2002, Nice, France*, 2002.

[3] J. Huang and J.A. Encinar. *Reflectarray Antennas.* IEEE Press Series on Electromagnetic Wave Theory. Wiley, 2007.

[4] Design optimization of reflectarrays. `http://www.ticra.com/products/consultancy/design-optimization-reflectarrays`. Accessed: 2015-07-30.

[5] Eduardo Carrasco, José Encinar, Mariano Barba, et al. Bandwidth improvement in large reflectarrays by using true-time delay. *Antennas and Propagation, IEEE Transactions on*, 56(8):2496–2503, 2008.

[6] Constantine A Balanis. *Antenna theory: analysis and design*, volume 1. John Wiley & Sons, 2005.

[7] Julien Perruisseau-Carrier. Microwave periodic structures based on microelectromechanical systems (mems) and micromachining techniques. *PhD. Thesis*, 2007.

[8] MJ Gans. A general proof of floquet's theorem (correspondence). *Microwave Theory and Techniques, IEEE Transactions on*, 13(3):384–385, 1965.

[9] José Encinar et al. Design of two-layer printed reflectarrays using patches of variable size. *Antennas and Propagation, IEEE Transactions on*, 49(10):1403–1410, 2001.

[10] José Encinar, J Agustin Zornoza, et al. Three-layer printed reflectarrays for contoured beam space applications. *Antennas and Propagation, IEEE Transactions on*, 52(5):1138–1148, 2004.

[11] Maurizio Bozzi, Simone Germani, and Luca Perregrini. Performance comparison of different element shapes used in printed reflectarrays. *Antennas and Wireless Propagation Letters, IEEE*, 2(1):219–222, 2003.

[12] Philippe Dreyer, Monica Morales-Masis, Sylvain Nicolay, Christophe Ballif, and Julien Perruisseau-Carrier. Copper and transparent-conductor reflectarray elements on thin-film solar cell panels. *Antennas and Propagation, IEEE Transactions on*, 62(7):3813–3818, 2014.

[13] JA Encinar, M Arrebola, M Dejus, and C Jouve. Design of a 1-metre reflectarray for dbs application with 15% bandwidth. In *Antennas and Propagation, 2006. EuCAP 2006. First European Conference on*, pages 1–5. IEEE, 2006.

[14] Harish Rajagopalan, Shenheng Xu, and Yahya Rahmat-Samii. On understanding the radiation mechanism of reflectarray antennas: An insightful and illustrative approach. *Antennas and Propagation Magazine, IEEE*, 54(5):14–38.

[15] David M Pozar, Stephen D Targonski, and HD Syrigos. Design of millimeter wave microstrip reflectarrays. *Antennas and Propagation, IEEE Transactions on*, 45(2):287–296, 1997.

[16] Maurizio Bozzi, Anthimos Georgiadis, and Kaijie Wu. Review of substrate-integrated waveguide circuits and antennas. *Microwaves, Antennas & Propagation, IET*, 5(8):909–920, 2011.

[17] David M Pozar. *Microwave engineering*. John Wiley & Sons, 2009.

[18] PW Hannan and MA Balfour. Simulation of a phased-array antenna in waveguide. *Antennas and Propagation, IEEE Transactions on*, 13(3):342–353, 1965.